NRC Research Press

ARTICLE

Spatiotemporal variation in size-structured populations using fishery data: an application to shortfin mako (*Isurus oxyrinchus*) in the Pacific Ocean[1]

Mikihiko Kai, James T. Thorson, Kevin R. Piner, and Mark N. Maunder

Can. J. Fish. Aquat. Sci. Downloaded from cdnsciencepub.com by NOAA CENTRAL on 06/05/23
For personal use only.

Abstract: We develop a length-disaggregated, spatiotemporal, delta-generalized linear mixed model (GLMM) and apply the method to fishery-dependent catch rates of shortfin mako sharks (*Isurus oxyrinchus*) in the North Pacific. The spatiotemporal model may provide an improvement over conventional time-series and spatially stratified models by yielding more precise and biologically interpretable estimates of abundance. Including length data may provide additional information to better understand life history and habitat partitioning for marine species. Nominal catch rates were standardized using a GLMM framework with spatiotemporal and length composition data. The best-fitting model showed that most hotspots for "immature" shortfin mako occurred in the coastal waters of Japan, while hotspots for "subadult and adult" occurred in the offshore or coastal waters of Japan. We also found that size-specific catch rates provide an indication that there has been a recent increasing trend in stock abundance since 2008.

Résumé : Nous développons un modèle spatiotemporel linéaire mixte généralisé (MLMG) par l'approche delta désagrégée selon la longueur et appliquons la méthode à des taux de prises dépendant de la pêche de requins-taupes bleus (*Isurus oxyrinchus*) dans le Pacifique Nord. Le modèle spatiotemporel pourrait constituer une amélioration par rapport aux séries chronologiques et aux modèles stratifiés dans l'espace classiques en produisant des estimations de l'abondance plus précises et facilement interprétables d'un point de vue biologique. L'inclusion de données sur la longueur pourrait fournir des renseignements supplémentaires pour mieux comprendre le cycle biologique et le partitionnement de l'habitat pour les espèces marines. Les taux de prises nominaux ont été normalisés en utilisant un cadre de MLMG avec des données spatiotemporelles et de composition selon la longueur. Le modèle présentant l'ajustement optimal montre que la plupart des points chaudes pour les requins-taupes bleus « immatures » sont dans les eaux littorales du Japon, alors que les points chauds pour les « subadultes et adultes » sont dans les eaux littorales ou au large du Japon. Nous avons également constaté que les taux de prises selon la taille indiquent une tendance récente d'augmentation de l'abondance du stock depuis 2008. [Traduit par la Rédaction]

Introduction

Reliable indices of population abundance are an important type of data for stock assessment (Francis 2011). For stocks lacking designed fishery-independent surveys, fishery catch-per-unit-effort (CPUE) data provide information on trends in stock abundance that is otherwise missing. Abundance indices provide not only trends, but can be used to estimate population scale when combined with catch in population dynamic models (Lee et al. 2014). Key to the use of these data are the assumption that the change in the index is proportional to changes in population abundance (Wilberg et al. 2010). Much attention has been devoted to estimation of CPUE from fishery-dependent catches and effort (Maunder and Punt 2004). Methods for standardizing CPUE data rely on introduction of auxiliary information to separate changes due to changing population abundance from those due to changes attributable to fishing practices and other factors. For widely dispersed stocks, the effects of spatial heterogeneity of both fish and fisheries need to be considered with respect to the assumption of proportionality between estimates of CPUE and population abundance. This becomes even more important when large areas of the stock distribution receive little or no effort, and assumptions about these areas becomes influential on estimates of stock trend (Walters 2003; Carruthers et al. 2010, 2011).

Spatiotemporal modeling methods have been introduced to deal with spatial variation in population distribution and density (e.g. Kai et al., in press; Petitgas et al. 2014; Roa-Ureta and Niklitschek 2007). Spatiotemporal modeling methods can be used to estimate population abundance indices using formal statistical tools such as likelihood functions and sampling designs (Kristensen et al. 2014; Thorson et al. 2015*b*, 2015*c*). Recent studies show that the approach may yield more precise, biologically reasonable, and interpretable estimates of abundance than common methods such as GLM (generalized linear model) and GLMM (generalized linear mixed model) (Shelton et al. 2014; Thorson et al. 2015*b*) by reducing sample selection bias and

Received 22 July 2016. Accepted 11 January 2017.

M. Kai. National Research Institute of Far Seas Fisheries (NRIFSF), Japan Fisheries Research and Education Agency, 5-7-1, Orido, Shimizu, Shizuoka 424-8633, Japan.
J.T. Thorson. Fisheries Resource Analysis and Monitoring Division, Northwest Fisheries Science Center, National Marine Fisheries Service (NMFS), NOAA, 2725 Montlake Boulevard E, Seattle, WA 98112, USA.
K.R. Piner. Southwest Fisheries Science Center, National Marine Fisheries Service (NMFS), NOAA, 8901 La Jolla Shores Drive, La Jolla, CA 92037, USA.
M.N. Maunder. Inter-American Tropical Tuna comission, 8604 La Jolla Shores Drive, La Jolla, CA 92037-1508, USA; Center for the Advancement of Population Assessment Methodology, Scripps Institution of Oceanography, La Jolla, CA 92093, USA.
Corresponding author: Mikihiko Kai (email: kaim@affrc.go.jp).

[1]This article is being published as part of the special issue "Space Oddity: Recent Advances Incorporating Spatial Processes in the Fishery Stock Assessment and Management Interface" arising from a related theme session at the 145th Annual Meeting of the American Fisheries Society, Portland, Oregon, USA, August 2015.

Copyright remains with the author(s) or their institution(s). Permission for reuse (free in most cases) can be obtained from RightsLink.

Can. J. Fish. Aquat. Sci. Downloaded from cdnsciencepub.com by NOAA CENTRAL on 06/05/23
For personal use only.

Table 1. Summary of the model selection information from (A) four analyses, including error distribution of positive catch model (lognormal or gamma), random field (anisotropic or isotropic), the number of parameters, the negative log-likelihood, the reduction in AIC (ΔAIC) from the best-fitting model, absolute value of the maximum gradient, marginal standard deviation for spatial variation, and spatiotemporal and length variation; and (B) eight analyses, including the catch rate predictor of random effect.

A. Four-model analysis.

Model	Error distribution of positive catch model	Random field	No. of parameters	Deviance	ΔAIC	Maximum gradient	Marginal SD of spatial variation	Marginal SD of spatiotemporal and length variation
Model A	Lognormal	Isotropic	30	88 261	53	0.065	0.243	1.217
Model B	Lognormal	Anisotropic	32	88 205	0	0.017	0.198	1.218
Model C	Gamma	Isotropic	30	89 434	1 226	0.005	0.240	1.221
Model D	Gamma	Anisotropic	32	89 383	1 179	0.038	0.207	1.225

B. Eight-model analysis.

Model	Catch rate predictors of random effect	No. of parameters	Deviance	Percent deviance (%)	ΔAIC	Maximum gradient	Marginal SD of spatial variation	Marginal SD of spatiotemporal and length variation
Model 1	Null	23	99 919		11 697	0.018		
Model 2	Station	27	98 741	1.179	10 527	0.019	0.59	
Model 3	Length	26	95 099	3.689	6 883	0.016		
Model 4	Station + Length	30	93 718	1.453	5 510	0.032	0.61	
Model 5	Station:Length:Year	29	88 504	5.564	293	0.067		1.84
Model 6	Station + Station:Length:Year	30	88 502	0.001	294	0.007	0.29	1.81
Model 7	Length + Station:Length:Year					0.145		
Model 8	Station + Length + Station:Length:Year	32	88 205	0.337	0	0.017	0.20	1.22

Note: "Null" denotes no random effects, "Station" denotes random effects of statistical station (latitude and longitude), "Length" denotes random effects of body length, and "Station:Length:Year" denotes random effects of station, length, and year.

filling in the spatial gaps common in fishery-dependent data (Carruthers et al. 2011; Thorson et al. 2016; Walter et al. 2014).

Spatial and temporal changes in the size (or age) structure of the population is an important aspect of the population abundance because marine fishes such as billfishes and oceanic pelagic sharks show evidence of spatial size (or age–stage) segregation (Nakano and Nagasawa 1996; Piner et al. 2013). Inclusion of auxiliary information about length into spatiotemporal methods allows prediction of the annual trends of the standardized CPUE by length, which may better account for changes in spatial patterns of size structure of the stock. Kristensen et al. (2014) developed a spatiotemporal dynamics model for Skagerrak cod (*Gadus morhua*), and Thorson et al. (2015*a*) developed a stage-structured model for rex sole (*Glyptocephalus zachirus*) in the Gulf of Alaska using information from different types of survey gear. These models incorporated size-structured information and described abundances of different size classes and spatial bycatch risk. It would be therefore useful to illustrate the temporal changes in the size-specific CPUE using the fishery-dependent data for pelagic sharks, which could be used to distinguish juvenile and nursery habitats for these species, similar to recent length-structured spatiotemporal analysis of survey trawls for shallow-water hake (*Merluccius capensis*) in the Benguela Current (Jansen et al. 2016).

Shortfin mako (*Isurus oxyrinchus*) is a large and highly migratory shark species and is widely distributed in the Pacific Ocean between 50°N and 50°S (Compagno 2001). Shortfin mako is susceptible to overexploitation due to slow growth rates, maturity at a late age, and low fecundity (Compagno 2001). Female shortfin mako attain maturity at a much larger size and older age (256 cm precaudal length (PCL), ~17 years old) than males (156 cm PCL, ~5 years old) (Semba et al. 2011). In the western and central North Pacific, mainly 60–240 cm PCL (0–20 years old) individuals are caught as bycatch by Japanese commercial pelagic longline fisheries targeting tuna and billfish (Kai et al. 2015). Standardized CPUE of shortfin mako in the North Pacific were estimated using the onboard observer data from 1995 to 2010; however, the historical trends of population abundance were poorly estimated due to the misspecification of the model (see Table 1; Clarke et al. 2013). Therefore, improvement of the estimates is needed to assess the status of shortfin mako stocks with greater accuracy and precision.

The objectives of this paper are to develop a length-disaggregated, spatiotemporal delta-GLMM using fishery-dependent catch-rate data and to apply the method to shortfin mako in the western and central North Pacific. This method is used to predict not only the temporal (yearly) changes in the CPUE but also the spatiotemporal distribution of CPUE for the different growth stages (size classes) of shortfin mako. Improvements in both standardized CPUE and understanding of spatial patterns of shortfin mako should result in better assessment and management of the stock.

Materials and methods

Data sources

Catch and effort data of Japanese shallow-set longliners operating in the western and central North Pacific from 2006 to 2014 were used to estimate the spatiotemporal variation in population density for shortfin mako in the last 9 years. We have a long time series of the catch and effort data from 1994 to 2014, but we used the data from 2006 to 2014 due to the limitation of the reliable length data. The set-by-set data used in this study included information on species of sharks, catch number, amount of effort (number of hooks), number of branch lines between floats (hooks between floats: HBF) as a proxy for gear configuration, and location (longitude and latitude) of set, with a resolution of 2° × 2° square. Only the shallow-set data were used in the analysis. The shallow-set data could be determined because fishermen changed the depth of the gear to change the target species, and the number of HBF varied depending on the depth (Nakano et al. 1997). We defined the shallow-set fishery by the use of a small number of HBF (i.e., 3–5). The hooks of the regular longline gear using these HBFs are estimated to hang at the depth around 50 to 120 m (Suzuki et al. 1977).

The National Research Institute of Far Seas Fisheries in Japan commenced a project to collect the length data of shortfin mako caught by Japanese coastal and offshore longline fishery in 2003.

Fig. 1. Map of the operational areas of Japanese commercial fisheries (mean number of hooks) and sampling areas of length data (length composition) in the western and central North Pacific. The map is drawn using the shallow-set fleet subset used for the analysis.

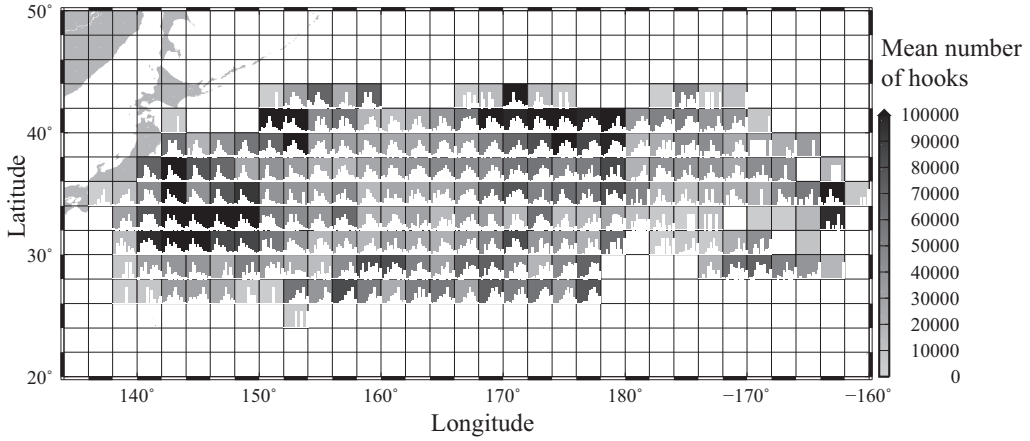

Can. J. Fish. Aquat. Sci. Downloaded from cdnsciencepub.com by NOAA CENTRAL on 06/05/23
For personal use only.

The fishermen in the Kesennuma fishing port measure the PCL of shortfin mako on the boat. The Kesennuma fishing port is located in the northeast part of the Japanese mainland, and it is well known for its large landings of tuna, billfish, and sharks (Ishimura and Bailey 2013). The longliner recorded the size and other auxiliary information such as sex and exact location of the starting position of each sets in addition to the information of the logbook data. We used the length data during 2006 and 2014 because many inaccurate records were included in the earlier periods during 2003 and 2005. The size data of each individual caught by shallow-set longliner was collated with the catch record of shortfin mako in the logbook of the longline boat with a resolution of 2° × 2° square and year and quarter. We then multiplied the catch rates from length-aggregated catch records by the proportion-at-size in the longliner logbook data and analysed these length-disaggregated catch rates. When a given 2° × 2° square did not have both longliner catch records and logbook data in a given quarter or year, we did not include that location in that time period in the model. Available data include the mean location and time of all sets with a resolution of 2° × 2° square and year and quarter. The detailed information about the data aggregation is summarized in Appendix A, Table A1).

The available data covered core areas of shortfin mako catch in the western and central North Pacific (24°N–44°N and 138°E–160°W; Fig. 1) and four seasons. Four seasons (quarters 1 to 4) were defined as follows: Q1 was spring (January to March); Q2 was summer (April to June); Q3 was fall (July to September); and Q4 was winter (October to December). The fishery data provide enough quantitative data to estimate the year-specific changes in the species distribution function and relative trends of CPUE for growth stages of shortfin mako in the western and central North Pacific. Three growth stages were defined as follows: "juvenile" denotes the body size smaller than 90 cm PCL (age-0); "immature" denotes the body size between 90 and 160 cm PCL; and "subadult and adult" denotes the body size larger than 160 cm PCL.

Spatiotemporal model with length composition data

Size and CPUE data originate from two different sampling processes, such that length measurement and catch per shot are not always directly matched. Then, the density estimate per station (i.e., grid cell) is informed by the CPUE data and then decomposed by the estimated contribution of each size class. The decomposition of the CPUE trend into individual size classes is the novel feature in this study. Previous studies that incorporated auxiliary length information into spatial and temporal models (Kristensen et al. 2014; Nielsen et al. 2014; Thorson et al. 2015*a*; Jansen et al. 2016) have focused on research trawl survey data based on underlying randomly stratified sampling designs, whereas we attempt to fit both length and CPUE to shallow-set longline fishery data. The fisheries-dependent data are collected from a highly unbalanced sampling design due to systematic changes in the spatial effort allocation and targeting behavior of the fleet (Carruthers et al. 2010, 2011; Thorson et al. 2016). A spatiotemporal modeling approach can in some cases account for fishery targeting occurring at large spatial scales and is therefore appropriate to account for some common forms of bias that arise when analyzing in fishery-dependent catch rates (Thorson et al. 2016).

We develop a model that accounts for both size-specific spatiotemporal variabilities in the distribution and the relative trends of catch rate of shortfin mako in the last 9 years in the western and central North Pacific. We use a length-structured spatiotemporal model for this task, so that we can explicitly decompose variance into additive components representing variation among years and size classes (Kristensen et al. 2014). We then use the model to predict density at unsampled locations, times, and length classes to provide a best-estimate of the distribution of species, relative trends of total abundance, and length compositions. Spatiotemporal and length modelling of CPUE data assumes that nearby locations and nearby size classes should have similar density estimates during each time interval. The correlation between statistical stations (latitude and longitude) and length classes (length bins) in a given interval is then used to estimate density in each year for all stations and length classes, including stations and length bins that do not have data in a given period. We then visualize the predictions of spatiotemporal variation in density and the temporal (yearly) changes in the total abundance for the different growth stages (size classes).

Model description

The spatiotemporal model incorporating length data estimated the density $d(s, t, q, l)$ in each station s (latitude and longitude with a resolution of 2° × 2° square), year t (where $t = 1$ signifies 2006 and $t = 9$ signifies 2014), quarter q (signifying a 3-month quarter, where $q = 1$ signifies Q1 (January–March) and $q = 4$ signifies Q4 (October–December)), and body length l (bin 1: 50–80 cm; bin 2: 80.1–90 cm; bin 3: 90.1–100 cm, …, bin 12: 180.1–190 cm; bin 13: 190.1–340 cm; e.g., where the first bin is all individuals less than or equal to 80 cm, and the last bin is all individuals greater than 190 cm). After estimating parameters, we then calculate juvenile density as the sum of density for 50–80 cm and 80.1–90 cm (i.e., the first and second length bins), immature as the sum of density for 90.1–100 cm to 150.1–160 cm (i.e., the third to ninth length bins), and subadult and adult as density for larger than 160.1 cm (i.e., the sum of the tenth to thirteenth length bins).

Can. J. Fish. Aquat. Sci. Downloaded from cdnsciencepub.com by NOAA CENTRAL on 06/05/23
For personal use only.

We modeled variation in density among both years and quarters to capture both annual trends in abundance and quarterly changes in catch rates. Each station, year, quarter, and length bin had density as follows:

$$(1)\qquad d(s,t,q,l) = \exp\Big[d_0(t) + \gamma(s) + \tau(l) + \theta(s,t,l) + \delta(q) + \sum_{j=1}^{n_j}\beta_j x_j(s,t,q,l)\Big]$$

where $d_0(t)$ represents intercept for year t, $\gamma(s)$ represents spatial variation (the mean density in station s relative to the average station), $\tau(l)$ represents the nonparametric impact of length on expected catch rates (the mean density in length l relative to the mean length), $\theta(s, t, l)$ represents an interaction term and spatiotemporal and length variation (variation in density for station s, year t, and length l after accounting for spatial, temporal, and length variation), $\delta(q)$ is an offset that represents the impact of quarter (q) on mean density, β_j is the effect of the jth covariate on predicted density, and $x_j(s, t, q, l)$ is the value of the jth covariate for a given location, year, quarter, and length category. In the following, we use as covariate the length of the individual (i.e., $n_j = 1$ and $x(s, t, q, l) = l$), which generates a log-linear increase or decrease in expected density with length, but future research could incorporate additional habitat variables. The marginal (common to all spatial stations and times) length variation, $\tau(l)$, is modeled using a first-order autoregressive process (AR1) to explain the correlations among length bins:

$$(2)\qquad \tau \sim \mathrm{MVN}\left(0, \sigma_\varepsilon^2 \mathbf{R}_\tau\right)$$

where MVN is a multivariate normal distribution with mean 0, correlation matrix $\mathbf{R}_\tau$, and pointwise variance σ_ε^2:

$$(3)\qquad \mathbf{R}_\tau(l, l') = \rho_\tau^{|l-l'|}$$

where ρ_τ is a parameter governing autocorrelation, while $|l - l'|$ is the difference in length among samples in length bin l and l'. ρ_τ is the magnitude of autoregression (where $\rho_\tau = 0$ implies that all lengths are statistically independent, while $\rho_\tau = 1$ implies that total density approaches a random-walk process among lengths). The model (eq. 1) includes both a parametric effect of length (by including a log-linear impact of length on expected catch using parameter β_j) and a nonparametric effect of length (by including a first-order autoregressive component using $\tau(l)$). We therefore interpret this as a "semiparametric" model with respect to the impact of length on catch rates (e.g., Kristensen 2014; Thorson and Taylor 2014).

Spatial variation $\gamma(s)$ is modeled as a Gaussian random field (GRF), which reduces to a multivariate normal distribution when evaluated at a finite set of stations (Thorson et al. 2015*c*):

$$(4)\qquad \gamma \sim \mathrm{MVN}(0, \Sigma_{\mathrm{spatial}})$$

where $\Sigma_{\mathrm{spatial}}$ is spatial covariance for the random field and approximated using a Matérn correlation function with smoothness $\nu = 1$:

$$(5)\qquad \Sigma_{\mathrm{spatial}}(s, s') = \frac{\sigma_\gamma^2}{\Gamma(\lambda)2^{\nu-1}}[\kappa|\mathbf{H}(s - s')|]^\nu K_\nu[\kappa|\mathbf{H}(s - s')|]$$

where $|s - s'|$ is the Euclidian distance between two generic locations s and s', σ_γ is the marginal variances of the spatial random field, Γ is the gamma function, and K_ν is the modified Bessel function of second kind (Lindgren et al. 2011). This covariance function calculates the correlation between γ at stations s and s' given their distance $|s - s'|$ after linear transformation $\mathbf{H}$, which accounts for geometric anisotropy (see supplementary data in Thorson et al. 2015*a*). If the spatial covariance structure is equivalent in all directions, it can be described as a function of distance only and is said to be isotropic (i.e., $\mathbf{H}$ is a two-dimensional identity matrix). If the spatial covariance structure varies in different directions, then it is a function of the distance and direction and is said to be anisotropic (where the directions of slow and fast decorrelation are given by $\mathbf{H}$). Isotropic processes form an inadequate basis in modelling many spatially distributed data, while $\mathbf{H}$ is essentially a linear transformation of coordinates as is common for estimating stationary anisotropy (Budrikaite and Ducinskas 2005). $\kappa > 0$ is a scaling parameter related to the range that means the distance at which the spatial correlation becomes almost null. We use a stochastic partial differential equation approximation to this function and can calculate the geostatistical range ($\sqrt{8\nu}/\kappa$) as the distance at which correlation is close to 10% for each smoothness parameter $\nu > 1/2$ (Lindgren et al. 2011). We used the Matérn correlation function because previous research demonstrated how the probability of GRFs could be calculated efficiently given this assumption (Diggle and Ribeiro 2007; Lindgren et al. 2011; Roa-Ureta and Niklitschek 2007). GRF is a convenient statistical approach for implementing a two-dimentional smoother for a response variable (in this case, catch) over spatial dimensions (Thorson et al. 2015*b*). The spatiotemporal and length variation, $\theta(s, t, l)$, is modeled by combining the GRF for spatial variation with first-order autoregressive process (AR1) for temporal and length variation:

$$(6)\qquad \boldsymbol{vec}(\boldsymbol{\theta_t}) \sim \mathrm{MVN}(0, \boldsymbol{\Sigma_{\mathrm{spatial}}} \otimes \mathbf{R_\theta})$$

where $\boldsymbol{vec}(\boldsymbol{\theta_t})$ is the vectorized value of $\theta(s, t, l)$ for all stations and length bins in year t, $\otimes$ is the Kronecker product where if $\mathbf{A}$ is an $m \times n$ matrix and $\mathbf{B}$ is a $p \times q$ matrix, then the Kronecker product $\mathbf{A} \otimes \mathbf{B}$ is the $mp \times nq$ block matrix:

$$(7)\qquad \mathbf{A} \otimes \mathbf{B} = \begin{bmatrix} \boldsymbol{a_{11}}\mathbf{B} & \cdots & \boldsymbol{a_{1n}}\mathbf{B} \\ \vdots & \ddots & \vdots \\ \boldsymbol{a_{m1}}\mathbf{B} & \cdots & \boldsymbol{a_{mn}}\mathbf{B} \end{bmatrix}$$

$\mathbf{R_\theta}$ is the correlation in θ_t among length bins

$$(8)\qquad \mathbf{R_\theta}(l, l') = \rho_\theta^{|l-l'|}$$

where ρ_θ is a parameter governing autocorrelation among length bins for the spatiotemporal variance component. In the following, $\delta(q)$ represents an increase or decrease in expected catch rates for each quarter relative to the first quarter ($\delta(1) = 0$ to ensure identifiability). We included both the covariate length as well as the AR1 for length variation, and we interpret this as a semiparametric specification of the effect of length on expected catch rates. We estimated a separate standard deviation for spatial (σ_γ) and spatiotemporal and length (σ_θ) components, but estimated the same decorrelation distance (κ) for the processes, using the implicit assumption that dynamics were defined by a "characteristic scale" that defined decorrelation distance for each of them. Following the parameterization from Lindgren et al. (2011), we estimated a magnitude parameter η for each spatial (η_γ) and spatiotemporal and length (η_θ) process and the corresponding standard deviation was then calculated as follows:

$$(9)\qquad \sigma_\gamma = 1\Big/\sqrt{\left(4\pi\eta_\gamma^2\right)}$$

where the other standard deviation (i.e., σ_θ) was calculated similarly (from η_θ). Aside from this, we also estimated a magnitude parameter η for length (η_τ) process.

Can. J. Fish. Aquat. Sci. Downloaded from cdnsciencepub.com by NOAA CENTRAL on 06/05/23
For personal use only.

Expected catch λ_i is a function of density and fishing effort f_i (number of hooks), $\lambda_i = d(s_i, t_i, q_i, l_i)f_i$, and is compared with the observed catch (in numbers) c_i for the ith observation in station s_i, year t_i, quarter q_i, and length l_i. Count data of the sharks typically included many observations with zero catch and a few observations with large values when the sharks were aggregated (Bigelow et al. 1999; Ward and Myers 2005). Population trends of bycatch species such as sharks are commonly estimated using the delta lognormal model to account for the occurrence of excess zeros (Lo et al. 1992; Zuur et al. 2009) and the negative binomial model or gamma model to account for overdispersion (Brodziak and Walsh 2013). The delta lognormal model is a combination of the probability of nonzero catches (encounter) assuming a logistic model and the probability of positive catch rates (catch rates for each encounter) assuming a lognormal model.

Because the compiled spatiotemporal data of shortfin mako showed evidence of excess zeros (51.3%) and the dispersion ratio (variance/mean = 34.9), we assume that available catch data c arises from the following delta (a.k.a., two stages) model, where the probability that a given sample is nonzero:

$$\Pr(C > 0) \equiv p = \left[\frac{1}{1 + \exp(-z_0)}\right][1 - \exp(-z_1\lambda)] \quad (10)$$

where z_0 governs the encounter probability given very high local densities (i.e., $p \to 1/[1 + \exp(-z_0)]$ as $\lambda \to \infty$), and z_1 governs how the probability of encounter increases with local expected catch λ. Catches then follow a lognormal distribution or a gamma distribution:

$$\Pr(C = c \mid c > 0) = \text{Lognormal}\left[C; \log\left(\frac{\lambda}{p}\right), \sigma^2\right] \quad (11)$$

$$\Pr(C = c \mid c > 0) = \text{Gamma}\left(C; \frac{1}{\text{CV}^2}, \frac{\lambda\text{CV}^2}{p}\right) \quad (12)$$

where Lognormal(x; m, σ^2) is the lognormal probability density function evaluated at x, given log-mean m and log-standard deviation σ, σ is the time-varying (i.e., yearly changes in) log-standard deviation for catch rates given an encounter, Gamma(x; α, β) is the probability density function of a gamma distribution with shape α and scale β, evaluated at x, CV is the coefficient of variation for catch rates given an encounter, and these equations are defined such that median (C) = λ.

Parameters representing temporal (year) variance (d_0), spatial covariance (κ and η_γ), length variance (ρ_τ and η_τ), spatiotemporal and length covariance (κ, ρ_θ, and η_θ), covariates of respective length (β) and quarter (δ), and residual variation (σ) were estimated as fixed effects while integrating across random effects representing spatial (station), length, and spatiotemporal and length variations (see Appendix A, Table A2). This integral was approximated using the Laplace approximation, and the fixed effects were estimated using gradient information as provided by Template Model Builder (TMB), which is an R package (R Core Team 2013) for fitting statistical latent variable models to data. It was inspired by ADMB (Fournier et al. 2012). The details of TMB are described by Kristensen et al. (2016). Further details regarding GRF estimation can be found in Thorson et al. (2015*b*, 2015*c*).

After estimating the fixed effects by maximizing the marginal likelihood of the data, the distribution of catch rates of shortfin mako were predicted from the random effects using empirical Bayes (i.e., by fixing them to the value that maximizes the joint likelihood with respect to random effects, while fixed effects are set to their maximum likelihood estimates; Appendix B). We used a recent bias-correction algorithm to account for retransformation bias when predicting and visualizing total abundance and size composition (Thorson and Kristensen 2016). Model convergence was confirmed by ensuring that the hessian matrix was positive definite and that the absolute value of the final gradient of parameters was less than 0.1.

Model selection and diagnostics

We selected the most parsimonious model using Akaike's information criterion (AIC; Akaike 1973) and percent deviation (Maunder and Punt 2004). AIC identifies which model had greater support given available data; this model selection is appropriate given that TMB implements maximum marginal likelihood estimation (Hoeting et al. 2006; Thorson et al. 2015*c*). Latter methodology examined a common ad hoc response that requires each addition of model complexity to explain more than some agreed minimum (0.5% was arbitrarily given) of additional percent deviation explained (Maunder and Punt 2004). First, we chose the best model with regards to the error distribution of the positive catch part in the zero-inflated model and the necessity of the anisotropy from the following four models:

Model A: delta-lognormal distribution model without anisotropy
Model B: delta-lognormal distribution model with anisotropy
Model C: delta-gamma distribution model without anisotropy
Model D: delta-gamma distribution model with anisotropy

where the full model in eq. 1 was used for these models. Second, we chose the best model with regards to the combinations of the explanatory variables for the selected model in the first model selection. We also compared the yearly changes in predicted catch rates among multiple models for first and second model selection. Coefficients of variation (CVs) and confidence intervals of annual changes in the CPUE were calculated for the best-fitting model using the information matrix and delta-method (Fournier et al. 2012). We also examined the standard regression diagnostic statistics for the best-fitting model to identify model misspecification and heteroscedasticity (Maunder and Punt 2004).

Results

The delta-lognormal distribution model with anisotropy and most complex model including temporal (quarter), spatial (station), length (precaudal length), and spatiotemporal and length variances as random effects was identified as the most parsimonious model by AIC (Table 1). Overall, the trend in predicted CPUE was almost similar among four models; however, the difference of the error distribution had a large impact on the trends in predicted CPUE in spite of the random field (Fig. 2*a*). The predicted CPUE was slightly changed if we added sequentially random effect components to the null model (Fig. 2*b*). These results and the marginal standard deviation (SD) in Table 1B indicated that the interaction terms and station had more impact on the changes in the trends than single length effect. Percent deviation also supported the result of the model selection by AIC (Table 1). We also examined the goodness-of-fits for the best-fitting model using residual diagnostics plots (Appendix C). We then used the best-fitting model to predict both the temporal (yearly) changes in the CPUE and also the spatiotemporal distribution of CPUE for the different growth stages of shortfin mako.

Mean overall spatial distribution of the predicted CPUE showed that most of the hotspots for shortfin mako were in the coastal (32°N–42°N and 136°E–146°E) and offshore (34°N–44°N and 150°E–170°E) waters of Japan (Fig. 3*a*). The predicted CPUE in offshore water tended to be lower than those in the coastal waters, with the highest CPUE found between 36°N–38°N and 142°E–144°E. The results were similar to the spatial distribution of the nominal CPUE except that the CPUE is generally higher at the northern boundary (Fig. 3*b*).

Predicted annual CPUE exhibited a slight decline to the lowest level in 2008 and then sharply increased until 2009 and increased again in 2014 (Fig. 4). Uncertainty in CPUE estimates is larger in the most recent years (2012–2014) than in the early years (2006–2008).

Can. J. Fish. Aquat. Sci. Downloaded from cdnsciencepub.com by NOAA CENTRAL on 06/05/23
For personal use only.

Fig. 2. Yearly changes in predicted catch per unit effort (CPUE) relative to its mean for shortfin mako for (*a*) four models with two different error distributions with and without anisotropy and (*b*) seven models with the explanatory variables sequentially added to the null model. See Appendix D for the calculation method of the quantity.

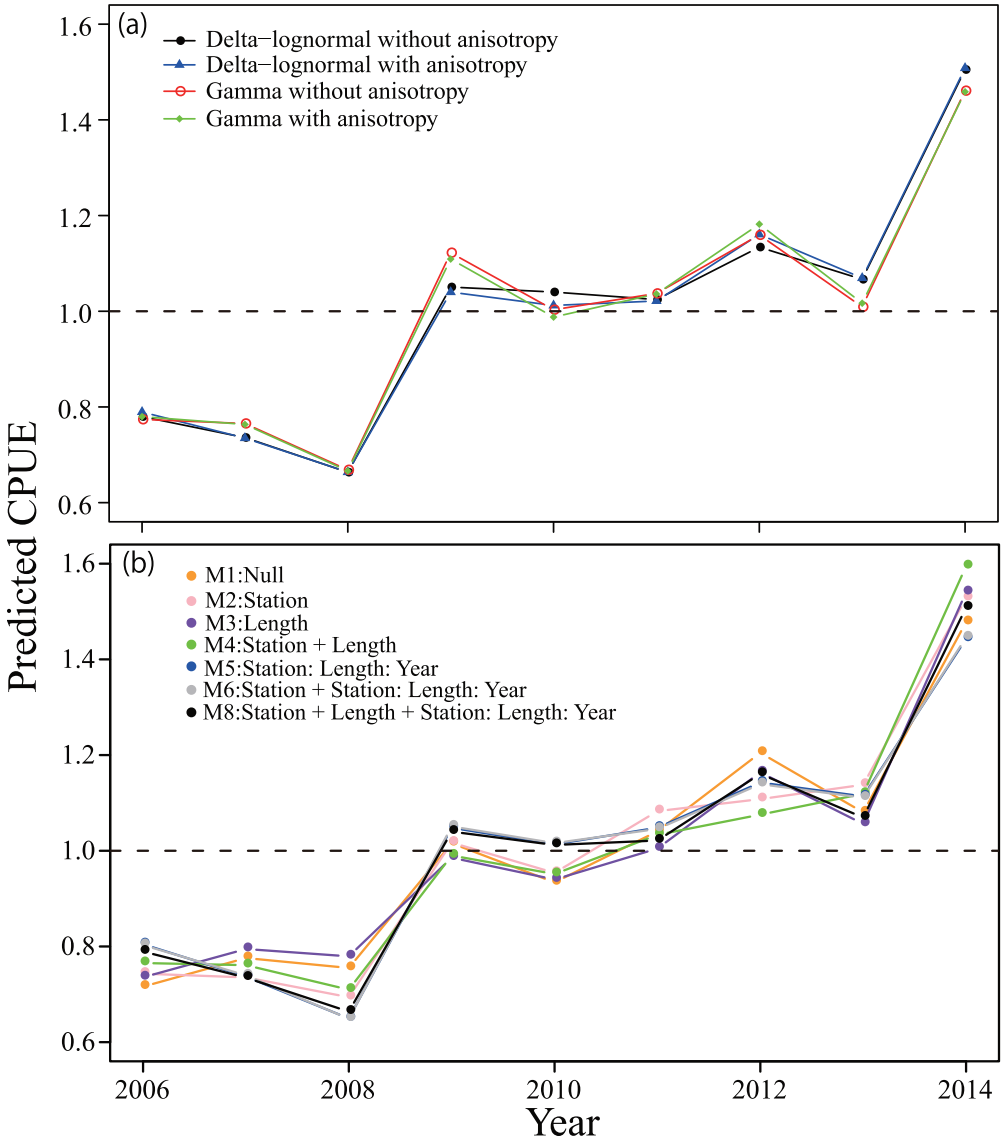

Predicted CPUE by PCL intervals (cm) was dome–shaped, with the highest CPUE peaking at 140 to 150 cm PCL (Fig. 5). This was a sharp contrast from the nominal peak in CPUE that occurred at 110 to 120 cm PCL. The overall mean length of predicted CPUE (146 cm PCL) was shifted to larger sizes compared with that of nominal CPUE (138 cm PCL) because the nominal CPUE by size class represented the pooled length weighted by the data (nominal catch divided by effort), and predicted CPUE by size class is weighted by area (predicted catch based on the spatial effect divided by effort). Uncertainty in CPUE estimates is larger in the middle ranges of the length classes (110–170 cm PCL) than both sides (smaller than 100 cm PCL and larger than 170 cm PCL).

The mean spatial distribution of the predicted CPUE for the three growth stages (Fig. 6) shows that most of the hotspots for juvenile shortfin mako (i.e., smaller than 90 cm PCL) were in the offshore waters off Japan (Fig. 6*a*), while most of the hotspots for immature shortfin mako (i.e., between 90 and 160 cm PCL) were in the coastal waters off Japan (Fig. 6*b*). Most of the hotspots for subadult and adult shortfin mako (i.e., larger than 160 cm PCL; Fig. 6*c*) were in the offshore waters of Japan, with some higher CPUE located in coastal waters (34°N–36°N and 138°E–142°E). The predicted CPUE hotspots were similar to those of nominal CPUE observations except that the nominal CPUE for juveniles was patchy (Figs. 6*d*–6*f*).

Yearly changes in the predicted CPUE for different growth stages are shown in Fig. 7 and Table D1. The values in Table D1 was calculated using the equations in Appendix D. Predicted CPUE of juvenile shortfin mako had a decreasing trend except in 2009 and 2014, and high CPUE were observed in 2006, 2009, and 2014 (Fig. 7*a*). The sharp increase in CPUE for juveniles from 2013 to 2014 was unlikely to occur for a low fecundity species like shortfin mako. Predicted CPUE of immature shortfin mako illustrated a slight decline to the lowest level in 2008 and then gradually increased and approached approximately 1.5 in 2014 (Fig. 7*b*). The trends in the CPUE time series is strongly similar to those for all size classes in Fig. 4 because Japanese shallow-set longline fishery dominantly catch the immature size classes between 90 and 160 cm PCL (see Fig. 5). The CVs of the predicted CPUE for immature shortfin mako were smaller than those for juvenile and subadult and adult shortfin mako (Table D1). Predicted CPUE of subadult and adult

Fig. 3. Overall spatial distribution of predicted CPUE relative its mean for shortfin mako (*a*), as well as the nominal CPUE relative to its mean (*b*). See Appendix D for the calculation method of the quantity.

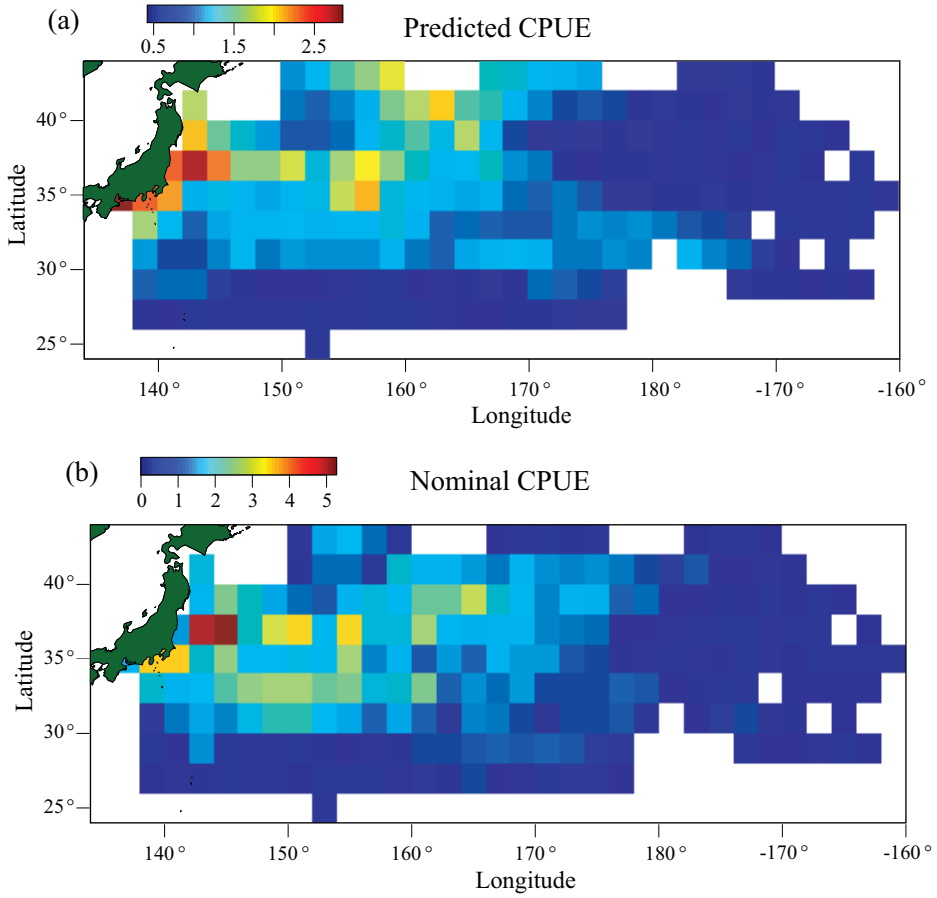

Fig. 4. Yearly changes in predicted CPUE relative its mean for shortfin mako (black solid line with circles). Grey solid line denotes the nominal CPUE relative to its mean, the shaded area denotes the 95% confidence intervals, and the horizontal dotted line denotes mean value of relative values (1.0). See Appendix D for the calculation method of the quantity.

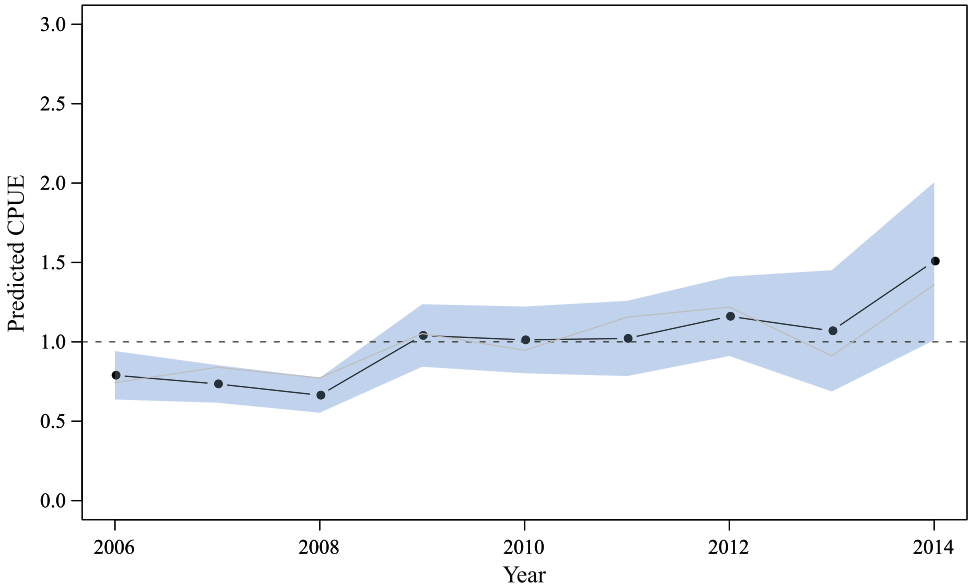

shortfin mako exhibited an increasing trend with larger CVs in accordance with the length of the elapsed time (Table D1). The fishing effort (number of hooks) showed a gradual decreasing trend since 2007, declining to approximately 0.5 million hooks in 2011 due to the Great East Japan Earthquake. Fishing effort increased in 2012 and maintained at approximately 0.75 million hooks until 2014.

The spatial distributions of the predicted CPUE for different growth stages showed that the locations of hotspots were not

Can. J. Fish. Aquat. Sci. Downloaded from cdnsciencepub.com by NOAA CENTRAL on 06/05/23
For personal use only.

Fig. 5. Length (precaudal)-specific changes in predicted CPUE relative to its mean for shortfin mako (black solid line with circles). Grey solid line denotes the nominal CPUE relative to its mean, the shaded area denotes the 95% confidence intervals, and the horizontal dotted line denotes mean value of relative values (1.0). See Appendix D for the calculation method of the quantity.

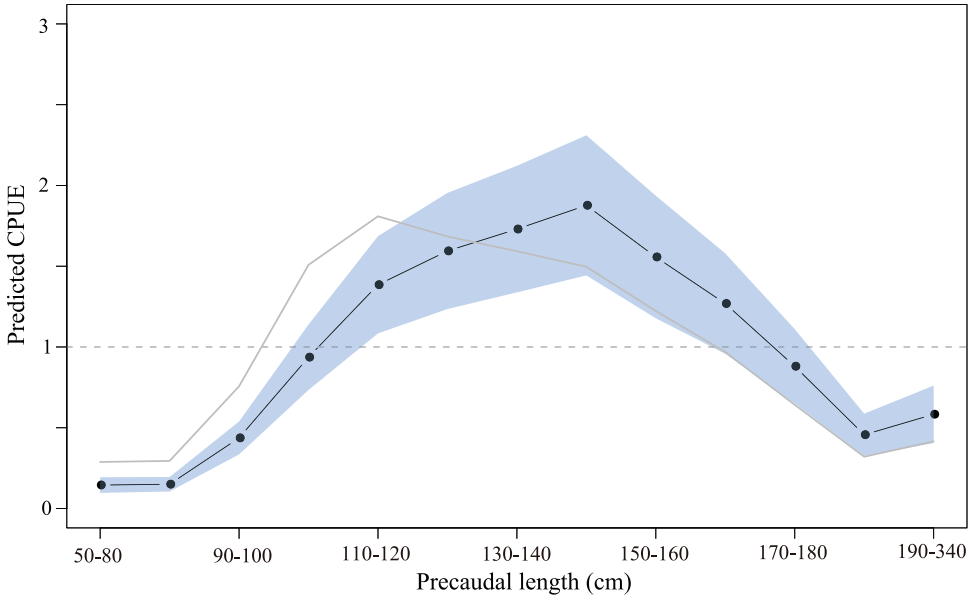

Fig. 6. Overall spatial distribution of predicted CPUE relative to its mean for three growth stages of shortfin mako: (*a*) juvenile, (*b*) immature, (*c*) subadult and adult. We also plot the nominal CPUE relative to its mean for the three growth stages of shortfin mako (*d*, *e*, *f*). See Appendix D for the calculation method of the quantity.

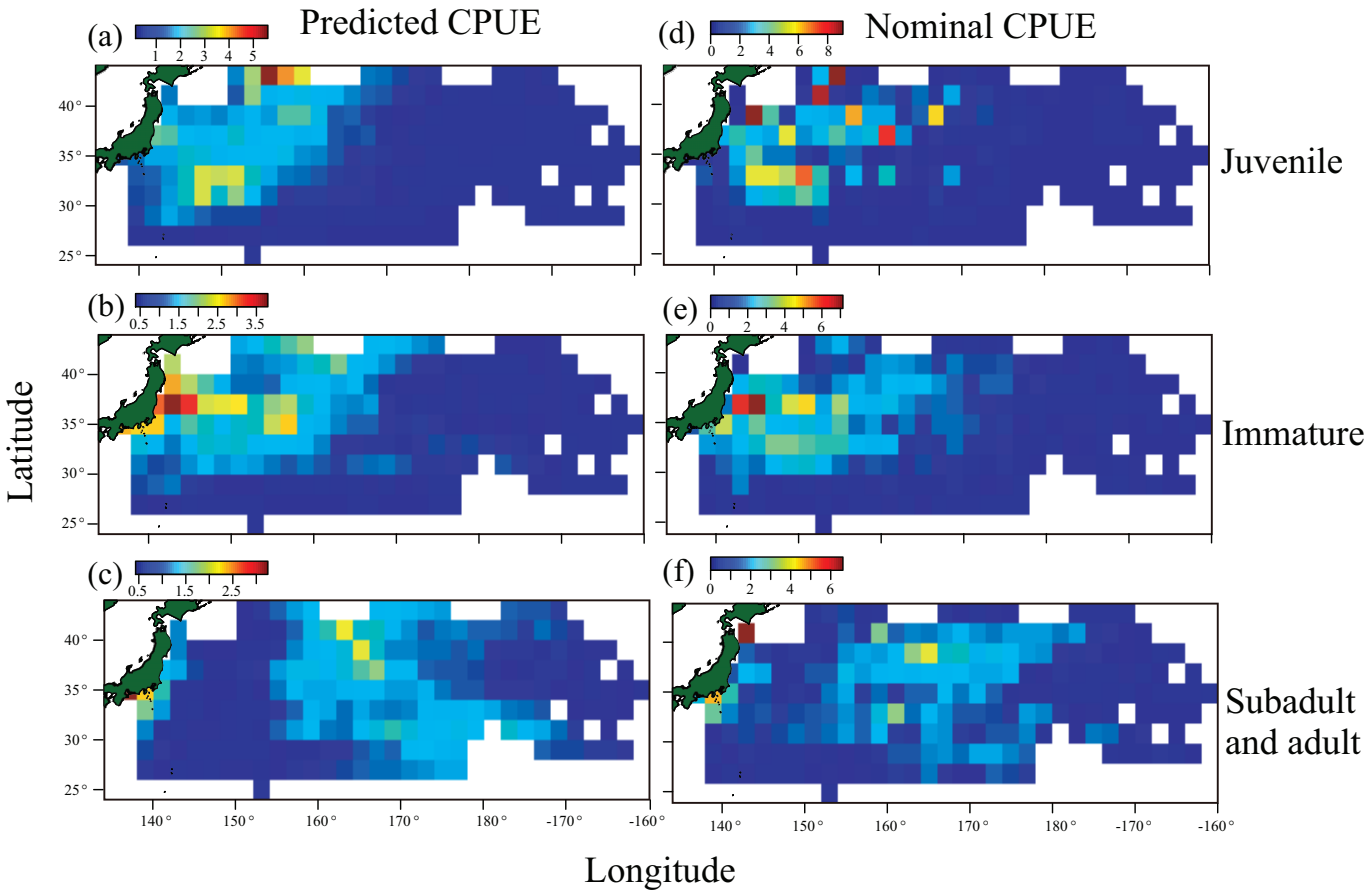

Can. J. Fish. Aquat. Sci. Downloaded from cdnsciencepub.com by NOAA CENTRAL on 06/05/23
For personal use only.

Fig. 7. Yearly changes in predicted CPUE relative to its mean (black solid line with circles) for three growth stages of shortfin mako: (*a*) juvenile, (*b*) immature, (*c*) subadult and adult. Grey solid line denotes the nominal CPUE relative to its mean for the three growth stages of shortfin mako, the shaded area denotes the 95% confidence intervals, and the horizontal dotted line denotes mean value of relative values (1.0). We also plot the number of hooks (× 1 million), representing the yearly changes of available data for shortfin mako (*d*). See Appendix D for the calculation method of the quantity.

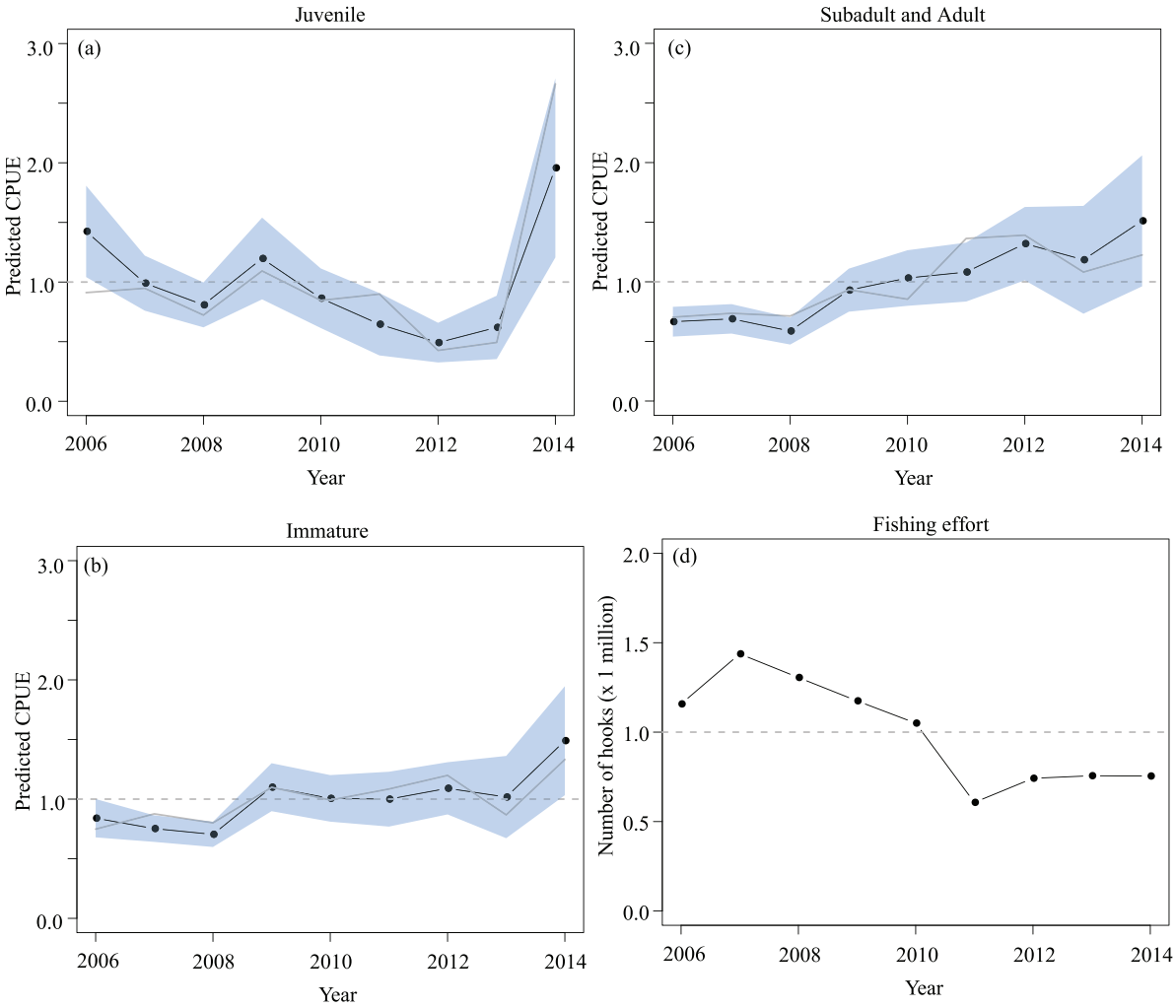

Can. J. Fish. Aquat. Sci. Downloaded from cdnsciencepub.com by NOAA CENTRAL on 06/05/23
For personal use only.

fixed through time (Fig. 8). Juvenile shortfin mako hotspots varied primarily latitudinally, with one instance of a coastal hotspot. For the others (i.e., immature, subadult and adult, all stages), annual variability in hotspots of CPUE was high and the numbers of hotspots were increased in more recent years than early years especially for the subadult and adult stage. During 2014 there was a particularly large hotspot for juveniles at the northern border, which probably caused the dramatic increase in the CPUE index for juveniles in that year.

Predicted CPUE by PCL (cm) showed similar dome shapes across years (Fig. 9). The years 2010 and 2013 were the most strongly peaked (at length bins from 140 to 150 cm PCL), with the other years estimated to have broader peaked CPUE (130–160 cm PCL).

Discussion

We developed a length-disaggregated, spatiotemporal, delta-generalized linear mixed model and applied the method to shortfin mako sharks in the North Pacific. Inclusion of auxiliary length data into the spatiotemporal model provided a tool to better understand life history and habitat partitioning for marine species such as shortfin mako shark.

Oceanic pelagic sharks such as a shortfin mako typically have relatively little reliable data because of the low economic values of these sharks compared with the more valuable species such as tuna and billfish (Bonfil 1994; Walker 1988). Because stocks of pelagic sharks are often data-poor (e.g., shortfin mako, which only has reliable length data starting in 2006), fishery indicators such as CPUE trends often provide the only information on stock status (ISC 2015). However, spatial shifts in fishing operations and the large spatial boundaries of stocks has made standardization of fishery catch rates problematic.

The spatiotemporal model used in this study predicted both density and length composition in areas where there is no data or inadequate data by explicitly considering the correlation of the data regarding the body length in addition to the space and time (Shelton et al. 2014; Thorson et al. 2015*b*). Thorson et al. (2015*b*) raised a concern about the spatiotemporal model that may result in biased estimates when fishing effort is correlated with population abundance (Diggle et al. 2010). However, the Japanese longline fishery does not target shortfin mako, so this may not be a problem. It is true that the spatiotemporal method will be subject to bias and increased variance if the hotspots of the shortfin mako overlaps with those of other target species, but this should also be true with more classical standardization methods.

In this study, we used a time-varying standard deviation for the statistical model. The fitting to the data could be better given a

Fig. 8. Time (year)-specific changes of the spatial distributions of log-scaled predicted CPUE for three growth stages and all combined stages of shortfin mako: juvenile, immature, subadult and adult, and all stages. See Appendix D for the calculation method of the quantity.

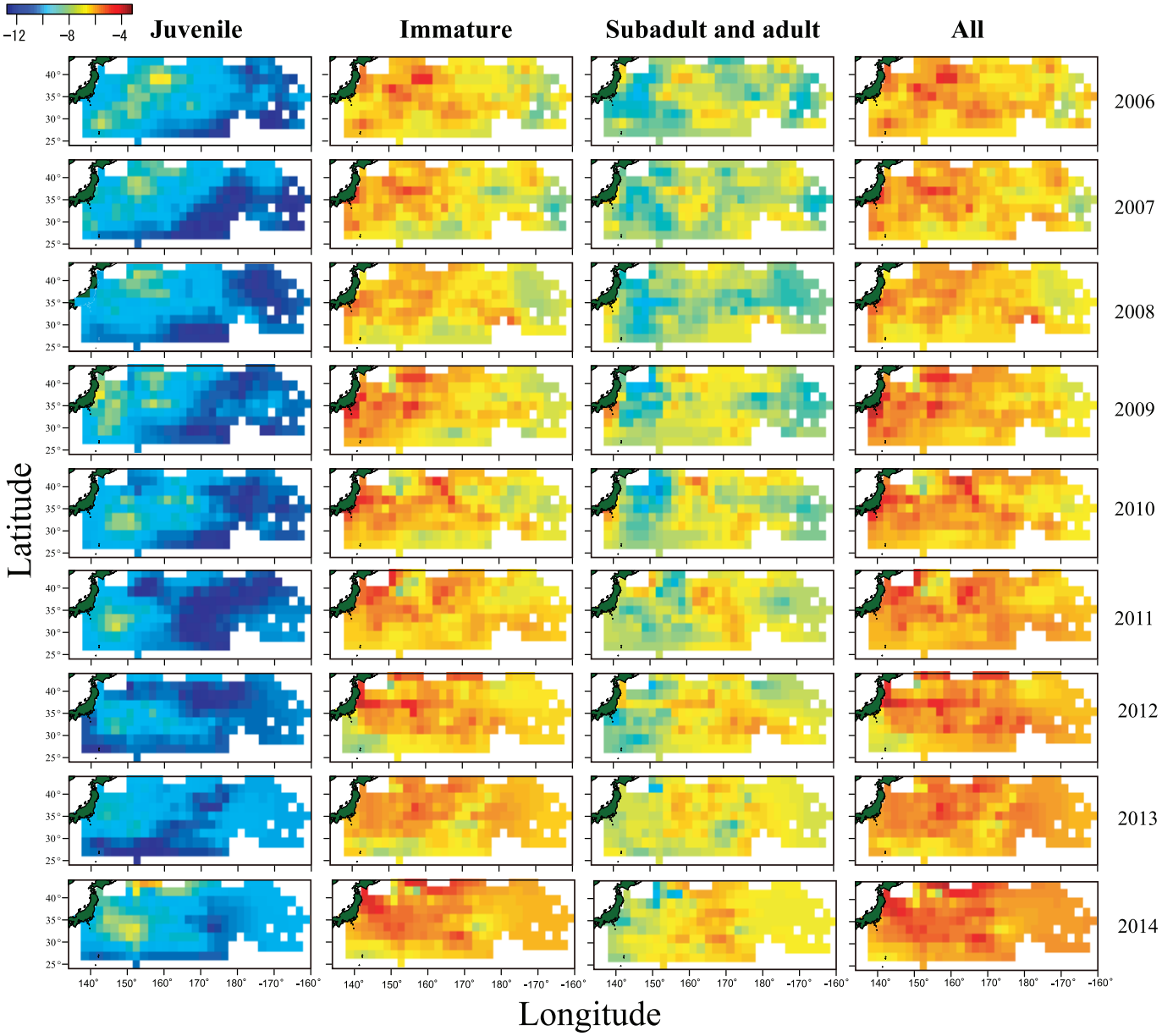

Can. J. Fish. Aquat. Sci. Downloaded from cdnsciencepub.com by NOAA CENTRAL on 06/05/23
For personal use only.

separate log-standard deviation for catch rates for each year because the observation errors fluctuate with changes in the operational patterns of the fishery for each year, although the number of the parameter is increased. In addition, it was shown that the inclusion of a stochastically time-varying common variance component can lead to substantial improvements in the fit of the time series (Bos and Koopman 2010).

Generalized linear mixed model commonly bases the AIC on the marginal model with the random effects integrated out, which may lead model selection to favor including more covariates than is optimal (Greven and Kneib 2010). Hoeting et al. (2006) demonstrated that the corrected AIC for a spatiotemporal model was superior to the standard approach of ignoring spatial correlation in the selection of explanatory variables. However, we used a standard AIC because the corrected AIC is similar to the standard AIC for large sample size.

In this modeling, we did not explicitly account for the differences in distribution or density between males and females because many records of length were associated with individuals for which the sex was not measured. Oceanic pelagic sharks such as a shortfin mako show evidence of remarkable sexual segregation in the estimated distribution (Mucientes et al. 2009), and sexual dimorphism also occurs (Bishop et al. 2006; Semba et al. 2009). Separately modelling spatiotemporal density for males and females would allow future analyses to identify differences in spatial distribution (and potentially different exploitation rates) for males and females as well as annual trends of the standardized catch rate by sex, and we recommend this line of future research. The spatiotemporal maps might provide the geographical segregation of species by sex from year to year and might be useful to identify the essential habitat such as pupping grounds and mating grounds. Ohshimo et al. (2016) reported that there was no strong evidence for sexual differences in the distribution patterns or environmental preferences for juvenile shortfin mako. However, their survey periods and areas are limited, so it is valuable to repeat those studies using more complete data in future work. Future spatiotemporal models could account for missing data

Can. J. Fish. Aquat. Sci. Downloaded from cdnsciencepub.com by NOAA CENTRAL on 06/05/23
For personal use only.

Fig. 9. Length-specific (precaudal) and time-specific (year) changes in predicted CPUE relative its mean for shortfin mako (black solid line with circles). Black solid line denotes the average length-specific distribution across all years, the shaded area denotes the 95% confidence intervals, and the horizontal dotted line denotes mean value of relative values (1.0). See Appendix D for the calculation method of the quantity.

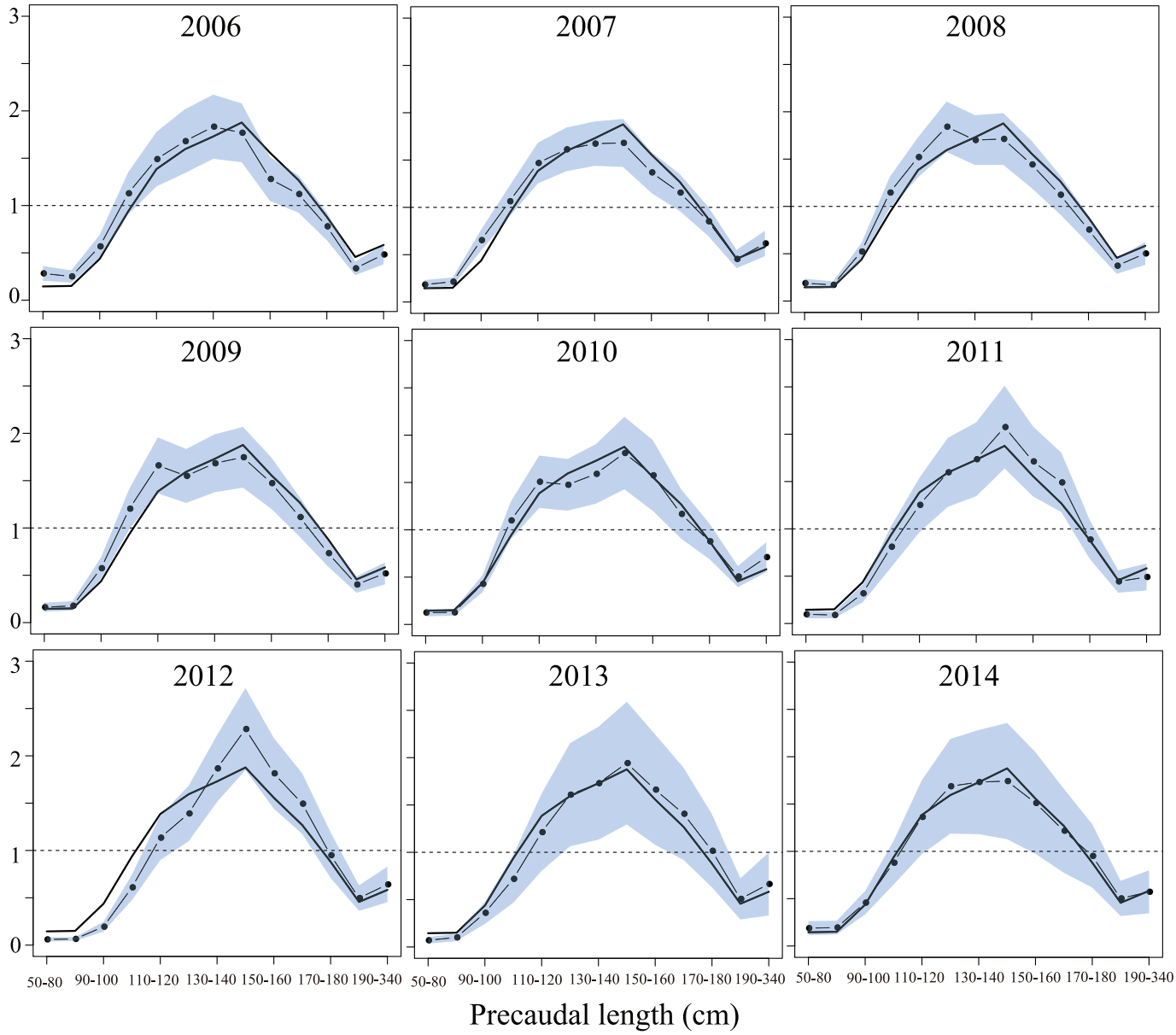

about individual sex by treating sex as a random effect (where observed catch rates follow a mixture distribution with two components). However, this requires prior information regarding the proportion by sex for each length category and would therefore require further model development.

The analysis we present is generally applicable and should be considered as a standard tool in fisheries stock assessment. CPUE data are typically standardized for factors such as area, season, and gear characteristics to develop indices of relative abundance, but the most common procedures (e.g., GLMs) give equal weight to each data point (Maunder and Punt 2004). However, since the index is supposed to represent the whole stock, the data may not be evenly spread over all areas biasing the index, and some form of area weighting should be used. The spatiotemporal approach automatically provides area weighting in addition to augmenting areas with no or little data (Thorson et al. 2015*b*). However, our approach takes this one step further to include length structure in the analysis. Despite CPUE data being standardized to produce an index of abundance, the accompanying composition data that is used to estimate the selectivity representing the index (i.e., the age or size of fish represented by the index) is not standardized or area-weighted. Use of our approach would harmonize the use of CPUE and composition data for creating indices of abundance for use in contemporary stock assessment models.

Hiraoka et al. (2016) reported that annual target shifts by Japanese shallow-set longliners occurred seasonally and geographically; the greatest change in target species, from swordfish (*Xiphias gladius*) to blue shark (*Prionace glauca*), occurred in spring (April–June). They used the 10th percentile of the swordfish CPUE values to incorporate this variable target behavior into the abundance index. We applied the same target indicator (rank of swordfish CPUE) to reduce the influences of the target behavior on the CPUE prediction of shortfin mako (Appendix E). The results indicated that the target changes between two target species had a small impact on the annual trends in the CPUE of shortfin mako (Fig. E1). Since shortfin mako shark is a bycatch species, unlike the

swordfish and blue shark, the target shifts may not largely influence on the trends in the CPUE.

We used state-of-the-art methods to standardize the catch and effort data, including extending the geostastical method to include length data. Three conclusions were derived from the application study: (1) most of the hotspots for "immature" shortfin mako (i.e., between 90 and 160 cm PCL) occurred in the coastal waters of Japan, while most of the hotspots for "subadults and adults" (i.e., larger than 160 cm PCL) occurred predominately in the offshore waters of Japan; (2) the predicted CPUE for the different growth stages provided an indication that the recent stock trends of shortfin mako in the western and central North Pacific was better than that in mid-2000s; (3) part of the juvenile population is probably outside the range of the fishery during some years, and therefore the CPUE-based index of abundance for juveniles is unreliable. Further research and testing of this promising approach is recommended towards making it a widely applicable standard tool for fisheries assessments.

Acknowledgements

We sincerely thank two anonymous reviewers and all members of the ISC shark Working Group that made invaluable comments and suggestions. We also appreciate Ko Shiozaki, who drew the clear map. We also thank Kasper Kristensen and the many contributors to the Template Model Builder software. We sincerely appreciate the crews of the coastal and offshore longline fleet from Kesennuma fishing port, Japan, for their full support in collecting samples from a wide range of the North Pacific. Finally, we are extremely grateful for the great contributions of Tadashi Oyama, Koshiro Ishida, Minoru Onodera, and Shigemitsu Onodera, who collected and measured the biological samples. This work was supported in part by a grant-in-aid from the Japan Fisheries Agency.

References

Akaike, H. 1973. Information theory as an extension of the maximum likelihood principle. *In* 2nd International Symposium on Information Theory. *Edited by* B.N. Petrov and F. Csaki. Akademiai Kiado, Budapest. pp. 267–281.

Bigelow, K.A., Boggs, C.H., and He, X. 1999. Environmental effects on swordfish and blue shark catch rates in the US North Pacific longline fishery. Fish. Oceanogr. **8**(3): 178–198. doi:10.1046/j.1365-2419.1999.00105.x.

Bishop, S.D.H., Francis, M.P., Duffy, C., and Montgomery, J.C. 2006. Age, growth, maturity, longevity and natural mortality of the shortfin mako shark (*Isurus oxyrinchus*) in New Zealand waters. Mar. Freshw. Res. **57**(2): 143–154. doi:10.1071/MF05077.

Bonfil, R. 1994. Overview of world elasmobranch fisheries. FAO Fish. Tech. Pap. 341.

Bos, C.S., and Koopman, S.J. 2010. Models with time-varying mean and variance: A robust analysis of U.S. industrial production. Tinbergen Institute Discusiion Paper, TI2010-017/4.

Brodziak, J., and Walsh, W.A. 2013. Model selection and multimodal inference for standardizing catch rates of bycatch species: a case study of oceanic whitetip shark in the Hawaii-based longline fishery. Can. J. Fish. Aquat. Sci. **70**(12): 1723–1740. doi:10.1139/cjfas-2013-0111.

Budrikaite, A., and Ducinskas, K. 2005. Modeling of geometric anisotropic spatial variation. *In* Proceeding of the 10th International Conference MMA2005& CMAM2, Trakai.

Carruthers, T.R., McAllister, M.K., and Ahrens, R.N.M. 2010. Simulating spatial dynamics to evaluate methods of deriving abundance indices for tropical tunas. Can. J. Fish. Aquat. Sci. **67**: 1409–1427. doi:10.1139/F10-056.

Carruthers, T.R., Ahrens, R.N.M., Mcallister, M.K., and Walters, C.J. 2011. Integrating imputation and standardization of catch rate data in the calculation of relative abundance indices. Fish. Res. **109**: 157–167. doi:10.1016/j.fishres.2011.01.033.

Clarke, S.C., Harley, S.J., Hoyle, S.D., and Rice, J.S. 2013. Population trends in Pacific oceanic sharks and the utility of regulations on shark finning. Conserv. Biol. **27**(1): 197–209. doi:10.1111/j.1523-1739.2012.01943.x.

Compagno, L.J.V. 2001. Sharks of the World. An annotated and illustrated catalogue of shark species known to date. Vol. 2. Bullhead, mackerel and carpet sharks (*Hetero dontiformes*, *Lamniforms* and *Orectolobiformes*). FAO Spes. Cat. Fish. Purp. 1(2), Rome, FAO.

Diggle, P., and Ribeiro, P. 2007. Model-Based Geostatics. Springer, New York.

Diggle, P.J., Menezes, R., and Su, T. 2010. Geostatistical inference under preferential sampling. J. R. Stat. Soc. Ser. C: Appl. Stat. **59**(2): 191–232. doi:10.1111/j.1467-9876.2009.00701.x.

Fournier, D.A., Skaug, H.J., Ancheta, J., Ianelli, J., Magnusson, A., Maunder, M.N., Nielsen, A., and Sibert, J. 2012. AD Model Builder: using automatic differentiation for statistical inference of highly parameterized complex nonlinear models. Optim. Methods Softw. **27**(2): 233–249. doi:10.1080/10556788.2011.597854.

Francis, R.I.C.C. 2011. Data weighting in statistical fisheries stock assessment models. Can. J. Fish. Aquat. Sci. **68**(6): 1124–1138. doi:10.1139/f2011-025.

Greven, S., and Kneib, T. 2010. On the behaviour of marginal and conditional AIC in linear mixed models. Biometrika, **97**(4): 773–789. doi:10.1093/biomet/asq042.

Hiraoka, Y., Kanaiwa, M., Ohshimo, S., Takahashi, N., Kai, M., and Yokawa, K. 2016. Relative abundance trend of the blue shark Prionace glauca based on the activities of Japanese distant water and offshore longliners in the North Pacific. Fish. Sci. **82**: 687–699. doi:10.1007/s12562-016-1007-7.

Hoeting, J.A., Davis, R.A., Merton, A.A., and Thompson, S.E. 2006. Model selection for geostatistical models. Ecol. Appl. **16**(1): 87–98. doi:10.1890/04-0576.

ISC. 2015. Indicator-based analysis of the status of shortfin mako shark in the north Pacific Ocean [online]. Report of the Shark Working Group. Kona, Hawaii, USA. Available from http://isc.fra.go.jp/pdf/ISC15/Annex%2012_SMA%20stock%20assessment%20report%20(2015)%2030Jul15_changes%20accepted.pdf [accessed 18 January 2017].

Ishimura, G., and Bailey, M. 2013. The market value of freshness: observations from the swordfish and blue shark longline fishery. Fish. Sci. **79**(3): 547–553. doi:10.1007/s12562-013-0609-6.

Jansen, T., Kristensen, K., Kainge, P., Durholtz, D., Strømme, T., Thygesen, U.H., Wilhelm, M.R., Kathena, J., Fairweather, T.P., Paulus, S., Degel, H., Lipinski, M.R., and Beyer, J.E. 2016. Migration, distribution and population (stock) structure of shallow-water hake (*Merluccius capensis*) in the Benguela Current Large Marine Ecosystem inferred using a geostatistical population model. Fish. Res. **179**: 156–167. doi:10.1016/j.fishres.2016.02.026.

Kai, M., Shiozaki, K., Ohshimo, S., and Yokawa, K. 2015. Growth and spatiotemporal distribution of juvenile shortfin mako, *Isurus oxyrinchus*, in the western and central North Pacific. Mar. Freshw. Res. **66**(12): 1176–1190. doi:10.1071/MF14316.

Kai, M., Thorson, J.T., Piner, K.R., and Maunder, M.N. Predicting the spatio-temporal distributions of pelagic sharks in the western and central North Pacific. [In press.] Fish. Oceanogr. doi:10.1111/fog.12217.

Kristensen, K. 2014. TMB: General random effect model builder tool inspired by ADMB [online]. R package version 1.6.2. Available from https://cran.r-project.org/web/packages/TMB/index.html [accessed 18 January 2017].

Kristensen, K., Thygesen, U.H., Andersen, K.H., and Beyer, J.E. 2014. Estimating spatio-temporal dynamics of size-structured populations. Can. J. Fish Aquat. Sci. **71**(2): 326–336. doi:10.1139/cjfas-2013-0151.

Kristensen, K., Nielsen, A., Berg, C.W., Skaug, H., and Bell, B.M. 2016. TMB: Automatic Differentiation and Laplace Approximation. J. Stat. Softw. **70**(5): 1–21. doi:10.18637/jss.v070.i05.

Lee, H.H., Piner, K.R., Methot, R.D., Jr., and Maunder, M.N. 2014. Use of likelihood profiling over a global scaling parameter to structure the population dynamics model: an example using blue marlin in the Pacific Ocean. Fish. Res. **158**: 138–146. doi:10.1016/j.fishres.2013.12.017.

Lindgren, F., Rue, H., and Lindström, J. 2011. An explicit link between Gaussian fields and Gaussian Markov random fields: The stochastic partial differential equation approach approach. J. R. Stat. Soc. Ser. B: Stat. Methodol. **73**(4): 423–498. doi:10.1111/j.1467-9868.2011.00777.x.

Lo, N.C., Jacobson, L.D., and Squire, J.L. 1992. Indices of Relative Abundance from Fish Spotter Data based on Delta-Lognormal Models. Can. J. Fish Aquat. Sci. **49**(12): 2515–2526. doi:10.1139/f92-278.

Maunder, M.N., and Punt, A.E. 2004. Standardizing catch and effort data: a review of recent approaches. Fish. Res. **70**(2–3): 141–159. doi:10.1016/j.fishres.2004.08.002.

Mucientes, G., Queiroz, N., Sousa, L., Tarroso, P., and Sims, D.W. 2009. Sexual segregation of pelagic sharks and the potential threat from fisheries. Biol. Lett. **5**(2): 156–159. doi:10.1098/RSBL.2008.0761.

Nakano, H., and Nagasawa, K. 1996. Distribution of pelagic elasmobranchs caught by salmon research gillnets in the North Pacific. Fish. Sci. **62**(6): 860–865. doi:10.2331/fishsci.62.860.

Nakano, H., Okazaki, M., and Okamoto, H. 1997. Analysis of catch depth by species for tuna longline fishery based on catch by branch lines. Bull. Natl. Rese. Inst. Far. Seas Fish. **34**: 43–62.

Nielsen, J.R., Kristensen, K., Lewy, P., and Bastardie, F. 2014. A Statistical Model for Estimation of Fish Density Including Correlation in Size, Space, Time and between Species from Research Survey Data. PLoS ONE, **9**(6): e99151. doi:10.1371/journal.pone.0099151.

Ohshimo, S., Fujinami, Y., Shiozaki, K., Kai, M., Semba, Y., Katsumata, N., Ochi, D., Matsunaga, H., Minami, H., Kiyota, M., and Yokawa, K. 2016. Distribution, body length, and abundance of blue shark and shortfin mako offshore of northeastern Japan, as determined from observed pelagic longline data, 2000-2014. Fish. Oceanogr. **25**(3): 259–276. doi:10.1111/fog.12149.

Petitgas, P., Doray, M., Huret, M., Masse, J., and Woillez, M. 2014. Modelling the variability in fish spatial distributions over time with empirical orthogonal functions: anchovy in the Bay of Biscay. ICES J. Mar. Sci. **71**(9): 2379–2389. doi:10.1093/icesjms/fsu111.

Piner, K.R., Lee, H.H., Kimoto, A., Taylor, I.G., Kanaiwa, M., and Sun, C.L. 2013. Population dynamics and status of striped marlin (*Kajikia audax*) in the western and central northern Pacific Ocean. Mar. Freshw. Res. **64**(2): 108–118. doi:10.1071/MF12302.

R Core Team. 2013. R: a language and environment for statistical computing. R Foundation for Statistical Computing, Vienna, Austria.

Can. J. Fish. Aquat. Sci. Downloaded from cdnsciencepub.com by NOAA CENTRAL on 06/05/23
For personal use only.

Roa-Ureta, R., and Niklitschek, E. 2007. Biomass estimation from surveys with likelihood based geostatistics. ICES J. Mar. Sci. **64**(9): 1723–1734. doi:10.1093/icesjms/fsm149.

Semba, Y., Nakano, H., and Aoki, I. 2009. Age and growth analysis of the shortfin mako, *Isurus oxyrinchus*, in the western and central North Pacific Ocean. Environ. Biol. Fish. **84**(4): 377–391. doi:10.1007/S10641-009-9447-X.

Semba, Y., Aoki, I., and Yokawa, K. 2011. Size at maturity and reproductive traits of shortfin mako, Isurus oxyrinchus, in the western and central North Pacific. Mar. Freshw. Res. **62**(1): 20–29. doi:10.1071/MF10123.

Shelton, A.O., Thorson, J.T., Ward, E.J., and Feist, B.E. 2014. Spatial semiparametric models improve estimates of species abundance and distribution. Can. J. Fish Aquat. Sci. **71**(11): 1655–1666. doi:10.1139/cjfas-2013-0508.

Suzuki, Z., Warashina, Y., and Kishida, M. 1977. The comparison of catches by regular and deep tuna longline gears in the western and central equatorial Pacific. Bull. Natl. Rese. Inst. Far. Seas Fish. **15**: 51–89.

Thorson, J.T., and Kristensen, K. 2016. Implementing a generic method for bias correction in statistical models using random effects, with spatial and population dynamics examples. Fish. Res. **175**: 66–74. doi:10.1016/j.fishres.2015.11.016.

Thorson, J.T., and Taylor, I.G. 2014. A comparison of parametric, semi-parametric, and non-parametric approaches to selectivity in age-structured assessment models. Fish. Res. **158**: 74–83. doi:10.1016/j.fishres.2013.10.002.

Thorson, J.T., Ianelli, J.N., Munch, S.B., Ono, K., and Spencer, P.D. 2015*a*. Spatial delay-difference models for estimating spatiotemporal variation in juvenile production and population abundance. Can. J. Fish. Aquat. Sci. **72**(12): 1897–1915. doi:10.1139/cjfas-2014-0543.

Thorson, J.T., Shelton, A.O., Ward, E.J., and Skaug, H. 2015*b*. Geostatistical delta-generalized linear mixed models improve precision for estimated abundance indices for West Coast groundfishes. ICES J. Mar. Sci. **72**: 1297–1310. doi:10.1093/icesjms/fsu243.

Thorson, J.T., Skaug, H., Kristensen, K., Shelton, A.O., Ward, E.J., Harms, J., and Benante, J. 2015*c*. The importance of spatial models for estimating the strength of density dependence. Ecology, **96**(5): 1202–1212. doi:10.1890/14-0739.1.

Thorson, J.T., Fonner, R., Haltuch, M., Ono, K., and Winker, H. 2016. Accounting for spatiotemporal variation and fisher targeting when estimating abundance from multispecies fishery data. Can. J. Fish. Aquat. Sci. **73**: 1–14. doi:10.1139/cjfas-2015-0598.

Walker, T.I. 1988. Can shark resources be harvested sustainably? A question revisited with a review of shark fisheries. Mar. Freshw. Res. **49**(7): 553–572. doi:10.1071/MF98017.

Walter, J.F., Hoenig, J.M., and Christman, M.C. 2014. Reducing bias and filling in spatial gaps in fishery-dependent catch-per-unit-effort data by geostatistical prediction, I. Methodology and simulation. N. Am. J. Fish. Manage. **34**(6): 1095–1107. doi:10.1080/02755947.2014.932865.

Walters, C. 2003. Folly and fantasy in the analysis of spatial catch rate data. Can. J. Fish Aquat. Sci. **60**(12): 1433–1436. doi:10.1139/f03-152.

Ward, P., and Myers, R.A. 2005. Shifts in open-ocean fish communities coinciding with the commencement of commercial fishing. Ecology, **86**(4): 835–847. doi:10.1890/03-0746.

Wilberg, M.J., Thorson, J.T., Linton, B.C., and Berkson, J. 2010. Incorporating time-varying catchability into population dynamic stock assessment models. Rev. Fish. Sci. **18**(1): 7–24. doi:10.1080/10641260903294647.

Zuur, A.E., Ieno, E.N., Walker, N.J., Saveliev, A.A., and Smith, G.M. 2009. Zero-truncated and zero-inflated models for count data. *In* Mixed effects models and extensions in ecology with R. Springer Science + Business Media, LLC, New York. pp. 261–293.

Appendix A

Basic statistical information about shortfin mako catch

The proportion of the catch number of mako shark caught by Japanese offshore and distant water shallow-set longliners accounts for approximately 93% (111 318/119 645) of the total catch by

Table A1. Summary of data aggregation by year and quarter.

	Catch number of mako shark		No. of size data		No. of set-by-set data		Positive catch ratio of set-by-set data		No. of hooks	
	Before	After	Before	After	Before	After	Before	After	Before	After
Year										
2006	13 180	10 299	7 800	7 648	5 123	3 200	0.57	0.53	18 583 512	15 319 327
2007	15 139	14 460	13 130	12 702	5 823	4 022	0.58	0.50	21 148 480	18 876 303
2008	12 532	12 080	10 571	10 113	5 312	3 610	0.61	0.52	19 185 566	17 139 978
2009	15 751	14 802	8 008	7 936	4 582	3 290	0.65	0.49	16 220 017	15 345 066
2010	13 202	11 907	6 282	6 238	4 181	2 702	0.64	0.48	15 388 103	13 785 927
2011	9 208	8 398	4 777	4 705	2 356	2 145	0.73	0.44	8 766 168	7 958 559
2012	11 202	10 833	6 918	6 841	2 900	2 473	0.66	0.51	10 506 429	9 710 781
2013	8 547	8 257	5 420	5 310	3 192	2 363	0.65	0.48	10 866 447	9 909 735
2014	12 557	12 292	9 449	9 389	3 072	2 231	0.75	0.57	10 216 910	9 838 298
Quarter										
1	33 729	32 561	21 908	21 605	10 785	5 633	0.69	0.54	37 990 354	36 575 575
2	30 343	26 183	16 598	16 084	9 191	8 753	0.64	0.44	33 049 087	29 311 644
3	20 075	19 053	14 399	14 158	6 222	5 442	0.69	0.49	22 511 714	20 889 069
4	27 171	25 531	19 450	19 035	10 343	6 208	0.53	0.56	37 330 477	31 107 685

Table A2. List of all parameters and the estimates for the best-fitting model.

Parameter name	Symbol	Type	Estimate
Distance of correlation (spatial random effect)	κ	Fixed	0.27
Northings anisotropy	h_1	Fixed	1.46
Anisotropic correlation	h_2	Fixed	0.98
Parameter governing pointwise variance (spatial random effect)	η_γ	Fixed	1.43
Parameter governing pointwise variance (length random effect)	η_τ	Fixed	0.30
Parameter governing pointwise variance (spatiotemporal and length random effect)	η_θ	Fixed	0.23
Correlation parameter of length bins	ψ	Fixed	0.17
Parameter governing autocorrelation (length random effect)	ρ_τ	Fixed	0.16
Parameter governing autocorrelation (spatiotemporal and length random effect)	ρ_θ	Fixed	0.85
Intercept for year	d_0	Fixed	Not shown
Temporal variance (quarter effect)[a]	δ	Fixed	Not shown
Scale parameter of zero catch ratio	z_1	Fixed	0.74
Scale parameter of zero catch ratio	z_0	Fixed	2.73
Log-standard deviation for catch rates for year	σ	Fixed	Not shown
Spatial residuals	γ	Random	Not shown
Length residuals	τ	Random	Not shown
Spatiotemporal and length residuals	θ	Random	Not shown

[a]Offset of density in quarters 2–4 from density in quarter 1.

Can. J. Fish. Aquat. Sci. Downloaded from cdnsciencepub.com by NOAA CENTRAL on 06/05/23
For personal use only.

Fig. A1. Maps of log-scaled nominal CPUE (catch/number of hooks ×1000) by station before and after the data aggregation. [Colour online.]

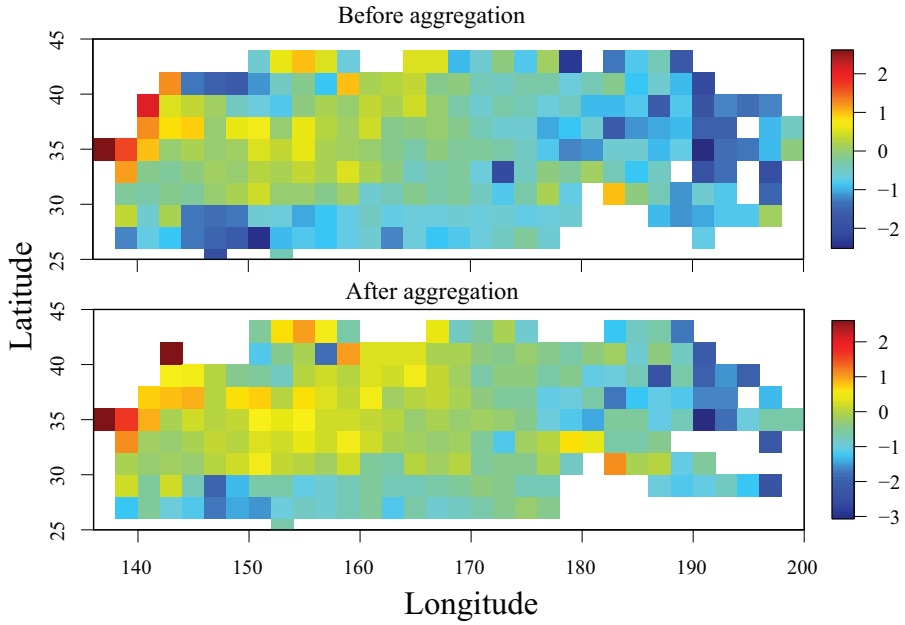

Can. J. Fish. Aquat. Sci. Downloaded from cdnsciencepub.com by NOAA CENTRAL on 06/05/23
For personal use only.

Japanese offshore and distant water longliners during 2006 and 2014 (if we defined the shallow-set fishery as having three to five hooks per float in an operation). Of this, the proportion of the catch number of mako shark caught by Kessennuma boats accounts for approximately 94% (104 864/111 318) of the total shallow-set catch during 2006 and 2014. Total number of size sample collected by Kesennuma boats was 72 355 during 2006 and 2014.

Summary of data aggregation

(1) For logbook catch data, we aggregated the set-by-set data (i.e., one operation data including year, quarter, latitude and longitude, number of hooks, catch number of shortfin mako and other species) by station (i.e., latitude and longitude) and year-quarter. Set-by-set data was summed up with regards to the catch number and number of hooks. There is no reduction in the total number of catch as well as hooks in this aggregation.

(2) For size data, we aggregated the set-by-set data (i.e., one operation data including year, quarter, latitude and longitude, body length of shortfin mako) by station, year-quarter, and length bins. Set-by-set data was summed up with regards to the total number of catch at each length interval. There is no reduction in the total number of size data.

(3) We combined the catch data with size data based on the same station and same year-quarter. If there is either (*i*) no size data at the specific station and in a specific year-quarter or (*ii*) no catch data at the specific station and in a specific year-quarter, then we do not include any data for that station and year-quarter. We summarized the information about the data aggregation in Table A1, and the maps of nominal CPUE before and after the data aggregation are depicted in Fig. A1. Note that the number of set-by-set data after aggregation denotes the number of data aggregated by station and year-quarter.

Appendix B

Estimation methods of the random effects (Kristensen et al. 2016)

Let $f(u, \omega)$ denote the negative joint log-likelihood of the data and the random effects. This depends on the unknown random effects $u \in R^n$ and parameters $\omega \in R^m$, where R is a real n- and m-space. The TMB package implements maximum likelihood estimation and uncertainty calculations for u and ω. The maximum likelihood estimate for ω maximizes

$$\text{(B1)} \qquad L(\omega) = \int_{R^n} \exp[-f(u, \omega)]du$$

with respect to ω. Note that the random effects u have been integrated out, and the marginal likelihood $L(\omega)$ is the likelihood of the data as a function of just the parameters. We use $\hat{u}(\omega)$ to denote the minimizer of $f(u, \omega)$ with respect to u; i.e.,

$$\text{(B2)} \qquad \hat{u}(\omega) = \arg\min_u f(u, \omega)$$

We use $H(\omega)$ to denote the Hessian of $f(u, \omega)$ with respect to u and evaluated at $\hat{u}(\omega)$; i.e.,

$$\text{(B3)} \qquad H_{i,j}(\omega) = \frac{\partial^2}{\partial \hat{u}_i(\omega)\partial \hat{u}_j(\omega)} f[\hat{u}(\omega), \omega]$$

The Laplace approximation for the marginal likelihood $L(\omega)$ is

$$\text{(B4)} \qquad L^*(\omega) = \sqrt{2\pi^n}\,\det[H(\omega)]^{-0.5}\exp[-f(u, \omega)]$$

We then use a gradient-based nonlinear minimizer to identify the values $\hat{\omega}$ of parameters ω that maximizes this approximation to the marginal likelihood:

$$\text{(B5)} \qquad \hat{\omega} = \arg\max_\omega L^*(\omega)$$

This approximation is widely applicable, including models ranging from nonlinear mixed effects models to complex space-time models.

Appendix C

Diagnostics plots of goodness-of-fits

The goodness-of-fits were examined using four types of residual plots obtained from positive catch data: (1) standardized residuals

Can. J. Fish. Aquat. Sci. Downloaded from cdnsciencepub.com by NOAA CENTRAL on 06/05/23
For personal use only.

Fig. C1. Diagnostic plots of goodness-of-fit for the most parsimonious model selected by AIC.

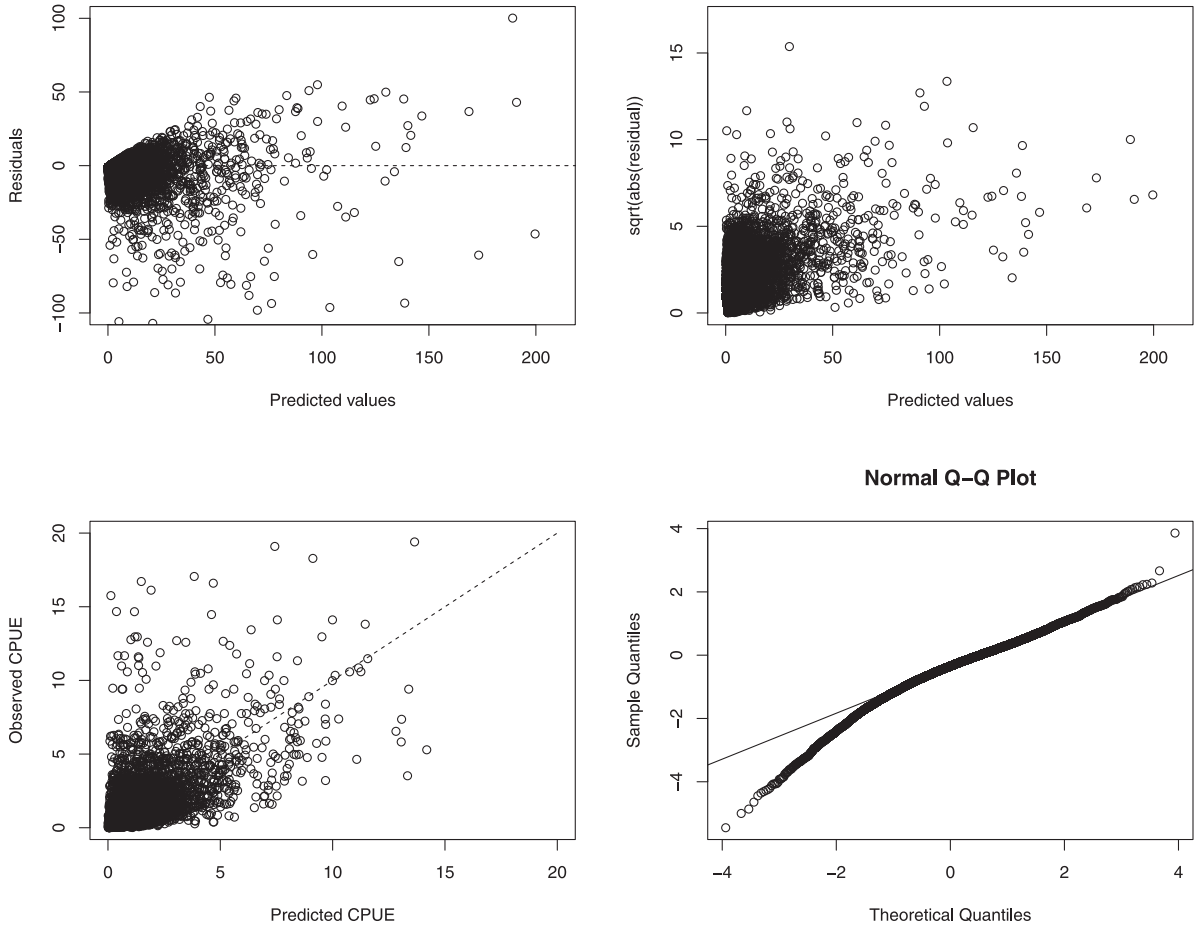

versus the fitted values can assess whether model misspecification is occurring; (2) square root of the absolute values of the standardized residuals versus the fitted values can assess whether the variance changes as a function of the predicted value; (3) the observed versus the predicted values can assess qualitatively whether the explanatory variables are indeed able to reduce the variance in the data; (4) quantile–quantile (Q–Q) plots can assess the normality. Overall, the model fit to the data was not bad (Fig. C1). The residuals were slightly biased toward the negative directions. Sqrt(Abs(Residuals)) had a tendency to increase as the predicted value was increased. The predicted CPUEs were smaller than observed CPUEs. Q–Q plots indicated that the left ends of the plots were largely deviated from the straight line.

We used only the positive catch data to plot the diagnostics because the binomial data with a logistic regression is very complicated to treat the residual patterns. If the true value is 0, we always overestimate the fitted value and the residual should be negative. If the true value is 1, we always underestimate the fitted value and the residual should be positive. Then, we have two lines of the residual plots across positive and negative lines.

Appendix D

Calculation method of each quantity

Annual abundance (i.e., CPUE, which is defined as catch number over number of hooks) is calculated as the sum of abundance for each station and length interval, averaged across quarter:

$$d(t) = \sum_{s=1}^{226}\sum_{l=1}^{13} d(s,t,q,l) \tag{D1}$$

where $d(s, t, q, l)$ is defined in eq. 1, and $d(t)$ is total abundance at year t. The overall year relative to its mean is

$$d^*(t) = d(t)\Big/\left[\frac{1}{n_t}\sum d(t)\right] \tag{D2}$$

Nominal CPUE for combined stations, length interval, and quarter is calculated as follows:

$$u(t) = \sum_{s=1}^{226}\sum_{q=1}^{4}\sum_{l=1}^{13} c(s,t,q,l)\Big/\sum_{s=1}^{226}\sum_{q=1}^{4}\sum_{l=1}^{13} f(s,t,q,l) \tag{D3}$$

where $u(t)$ is nominal CPUE at year t defined by a division of catch number c averaged over s, q, and l divided by number of hooks f averaged over s, q, and l. The overall year relative to its mean is

$$u^*(t) = u(t)\Big/\left[\frac{1}{n_t}\sum u(t)\right] \tag{D4}$$

The coefficient of variation (CV) for estimated CPUE for combined three growth stages in year t is calculated as follows:

$$CV[d(t)] = \frac{SE[d(t)]}{d(t)} \tag{D5}$$

where $CV[d(t)]$ is the coefficient of variation of total abundance in year t, and $SE[d(t)]$ is the standard error for annual abundance (as estimated using TMB).

Table D1. Summary of yearly changes in CPUE predicted by spatiotemporal model for three growth stages (juvenile, immature, and subadult and adult) and a combined stage (all) along with the corresponding estimates of the coefficient of variation (CV) and yearly changes in the nominal CPUE and fishing effort (number of hooks × 1 million).

	Predicted				Nominal				CV				Effort
Year	All	Juvenile	Immature	Adult	All	Juvenile	Immature	Adult	All	Juvenile	Immature	Adult	All
2006	0.79	1.42	0.84	0.67	0.74	0.91	0.75	0.70	0.10	0.14	0.10	0.10	0.10
2007	0.73	0.99	0.75	0.69	0.84	0.95	0.88	0.74	0.08	0.12	0.08	0.09	0.08
2008	0.66	0.81	0.70	0.59	0.77	0.72	0.80	0.71	0.08	0.12	0.08	0.10	0.08
2009	1.04	1.20	1.10	0.93	1.05	1.09	1.10	0.93	0.09	0.15	0.09	0.10	0.10
2010	1.01	0.86	1.01	1.03	0.95	0.85	0.99	0.85	0.10	0.15	0.10	0.12	0.11
2011	1.02	0.65	1.00	1.08	1.16	0.90	1.08	1.36	0.12	0.21	0.12	0.12	0.12
2012	1.16	0.49	1.09	1.32	1.22	0.43	1.20	1.39	0.11	0.17	0.10	0.12	0.11
2013	1.07	0.62	1.02	1.18	0.91	0.49	0.87	1.08	0.18	0.22	0.17	0.19	0.18
2014	1.51	1.96	1.49	1.51	1.36	2.66	1.33	1.22	0.17	0.20	0.16	0.19	0.17

Note: The values are predicted using the best-fitting model and scaled by mean CPUE.

Length-specific changes in abundance are calculated as the sum of abundance for each station and year, averaged across quarter:

$$d(l) = \sum_{s=1}^{226}\sum_{t=1}^{9} d(s,t,q,l) \quad \text{(D6)}$$

where $d(s, t, q, l)$ is defined in eq. 1, and $d(l)$ is total abundance at length bin l. The overall length interval relative to its mean is

$$d^*(l) = d(l)\Big/\left[\frac{1}{n_l}\sum d(l)\right] \quad \text{(D7)}$$

Nominal CPUE for combined stations, overall year, and quarter is calculated as follows:

$$u(l) = \sum_{s=1}^{226}\sum_{q=1}^{4}\sum_{t=1}^{9} c(s,t,q,l)\Big/\sum_{s=1}^{226}\sum_{q=1}^{4}\sum_{t=1}^{9} f(s,t,q,l) \quad \text{(D8)}$$

where $u(l)$ is nominal CPUE at length interval l defined by a division of catch number c averaged over s, q, and t divided by number of hooks f averaged over s, q, and t. The overall length interval relative to its mean is

$$u^*(l) = u(l)\Big/\left[\frac{1}{n_l}\sum u(l)\right] \quad \text{(D9)}$$

The CV for estimated CPUE at length interval l is calculated as follows:

$$\mathrm{CV}[d(l)] = \frac{\mathrm{SE}[d(l)]}{d(l)} \quad \text{(D10)}$$

where CV[$d(l)$] is the coefficient of variation of total abundance at length interval l, and SE[$d(l)$] is the standard error for annual abundance (as estimated using TMB).

In our study, we presented and interpreted maps of density that include the effect of fixed effects and random effects. Here, the mean spatial distribution of predicted catch rate for each year was calculated as follows:

$$\bar{d}(s,t) = \sum_{l=1}^{13} d(s,t,q,l) \quad \text{(D11)}$$

where $d(s, t, q, l)$ is defined in eq. 1, $\bar{d}(s, t)$ (the density at location s and time t summed over length intervals l is 13), the sum of quarter q is omitted because q is a fixed effect with no interactions, and the overall station relative to its mean is

$$d_t^*(s) = \frac{d(s,t)}{\left[(1/n_s)\sum d(s,t)\right]} \quad \text{(D12)}$$

Fig. E1. Yearly changes in predicted CPUE relative its mean for shortfin mako with target effect (solid line with circles) and without target effect (solid line with triangles). Target effect (Hiraoka et al. 2016) is defined as a ranking of swordfish catch ratio (i.e., CPUE for each set) based on ten equal percentile categories (e.g., 0% to <10%, 10% to <20%, etc.) for each year. Grey solid line denotes the nominal CPUE relative to its mean, and the horizontal dotted line denotes mean value of relative values (1.0).

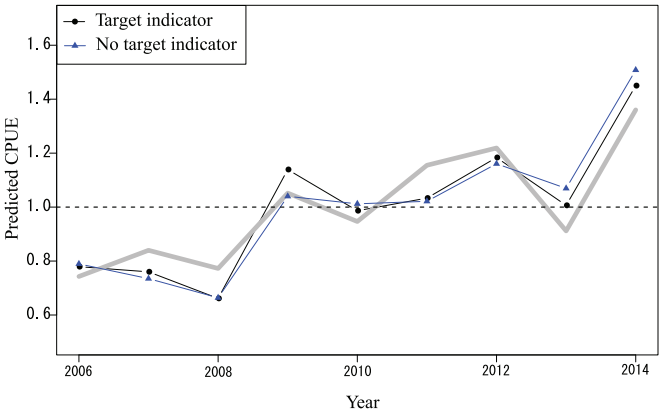

Appendix E

Influence of the target changes

Swordfish catch ratios (i.e., CPUE) were ranked based on ten equal percentile categories (e.g., 0% to <10%, 10% to <20%, etc.) for each year, and the ranks were used as target indicators (Hiraoka et al. 2016). We used the catch number records for swordfish and blue shark from the same set-by-set logbook data as used for the prediction of the CPUE for shortfin mako. We evaluated the influence of the target changes through a comparison with the annual trends in the CPUE using the best-fitting model with and without target indicator. For example, a set with the highest swordfish CPUE within certain years would be categorized as rank 10, indicating that blue shark was relatively under-targeted in that set.

References

Hiraoka, Y., Kanaiwa, M., Ohshimo, S., Takahashi, N., Kai, M., and Yokawa, K. 2016. Relative abundance trend of the blue shark *Prionace glauca* based on Japanese distant-water and offshore longliner activity in the North Pacific. Fish. Sci. **82**: 687–699. doi:10.1007/s12562-016-1007-7.

Kristensen, K., Nielsen, A., Berg, C.W., Skaug, H., and Bell, B.M. 2016. TMB: Automatic Differentiation and Laplace Approximation. J. Stat. Softw. **70**(5): 1–21. doi:10.18637/jss.v070.i05.

Can. J. Fish. Aquat. Sci. Downloaded from cdnsciencepub.com by NOAA CENTRAL on 06/05/23
For personal use only.